THE JOURNAL OF PHYSICAL CHEMISTRY A

 VOLUME 112, NUMBER 17, MAY 1, 2008

FEATURE ARTICLE

Control of Molecular Fragmentation Using Shaped Femtosecond Pulses

Vadim V. Lozovoy, Xin Zhu, Tissa C. Gunaratne, D. Ahmasi Harris, Janelle C. Shane, and Marcos Dantus*

Department of Chemistry and Department of Physics and Astronomy, Michigan State University, East Lansing, Michigan 48824

Received: March 1, 2007; In Final Form: February 7, 2008

The possibility that chemical reactions may be controlled by tailored femtosecond laser pulses has inspired recent studies that take advantage of their short pulse duration, comparable to intramolecular dynamics, and high peak intensity to fragment and ionize molecules. In this article, we present an experimental quest to control the chemical reactions that take place when isolated molecules interact with shaped near-infrared laser pulses with peak intensities ranging from 10^{13} to 10^{16} W/cm^2. Through the exhaustive evaluation of hundreds of thousands of experiments, we methodically evaluated the molecular response of 16 compounds, including isomers, to the tailored light fields, as monitored by time-of-flight mass spectrometry. Analysis of the experimental data, taking into account its statistical significance, leads us to uncover important trends regarding the interaction of isolated molecules with an intense laser field. Despite the energetics involved in fragmentation and ionization, the integrated second-harmonic generation of a given laser pulse (I_{SHG}), which was recorded as an independent diagnostic parameter, was found to be linearly proportional to the total ion yield (I_{MS}) generated by that pulse in all of our pulse shaping measurements. Order of magnitude laser control over the relative yields of different fragment ions was observed for most of the molecules studied; the fragmentation yields were found to vary monotonically with I_{MS} and/or I_{SHG}. When the extensive changes in fragmentation yields as a function of I_{MS} were compared for different phase functions, we found essentially identical results. This observation implies that fragmentation depends on a parameter that is responsible for I_{MS} and independent from the particular time−frequency structure of the shaped laser pulse. With additional experiments, we found that individual ion yields depend only on the average pulse duration, implying that coherence does not play a role in the observed changes in yield as a function of pulse shaping. These findings were consistently observed for all molecules studied (*p*-, *m*-, *o*-nitrotoluene, 2,4-dinitrotoluene, benzene, toluene, naphthalene, azulene, acetone, acetyl chloride, acetophenone, *p*-chrolobenzonitrile, *N*,*N*-dimethylformamide, dimethyl phosphate, 2-chloroethyl ethyl sulfide, and tricarbonyl-[η5-1-methyl-2,4-cyclopentadien-1-yl]-manganese). The exception to our conclusion is that the yield of small singly-charged fragments resulting from a multiple ionization process in a subset of molecules, were found to be highly sensitive to the phase structure of the intense pulses. This coherent process plays a minimal role in photofragmentation; therefore, we consider it an exception rather than a rule. Changes in the fragmentation process are dependent on molecular structure, as evidenced in a number of isomers, therefore femtosecond laser fragmentation could provide a practical dimension to analytical chemistry techniques.

I. Introduction

The quest for controlling chemical reactions with lasers is one fraught with dreams, breakthroughs, and disappointments. It involves a complex time-dependent interaction between light and matter in which energy redistribution and decoherence play a significant role. With some stretch of the imagination, we could pick as our first reference Hesiod's *Theogony* dating as far back as 700 BC where the struggles of the Greek gods of

* To whom correspondence should be addressed. E-mail: dantus@msu.edu.

10.1021/jp071691p CCC: $40.75
Published on Web 04/24/2008

Vadim V. Lozovoy received his Ph.D. degree from Novosibirsk State University (Russia). As a researcher at the Academy of Science of USSR, he worked on radiation chemistry, photochemistry and femtosecond spectroscopy. In 1998, he moved to the U.S.A. as a Research Associate and later as a Research Professor. He is currently an Academic Specialist at Michigan State University. His research interests now include laser control of chemical reactions and nonlinear multiphoton spectroscopy using phase-modulated femtosecond lasers. He has more than 100 publications and a few patents.

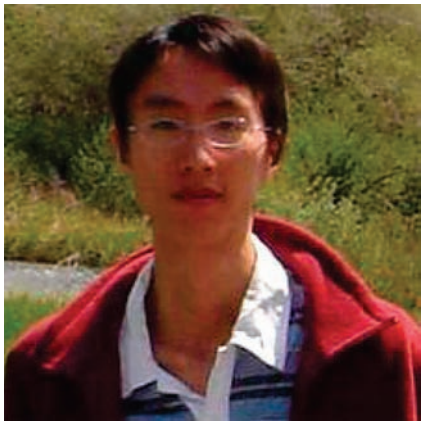

Xin Zhu received his B.A. degree of Chemistry from Peking University (China). In 2005, he came to Michigan State University and is currently pursuing his Ph.D, under the direction of Professor Marcos Dantus. The goal of his research is to understand the fundamentals of laser-induced molecular fragmentation and use this understanding to control molecular reactivity.

Tissa C. Gunaratne was born in Sri Lanka. He received his B.Sc. in Chemistry from the University of Sri Jayewardanepura, Sri Lanka, in 1995 and a Ph.D. in Photochemical Sciences from Bowling Green State University, Ohio, in 2003. For 2 years, he worked as a postdoctoral researcher on femtosecond time-resolved Raman experiments at Case Western Reserve University. Currently, he is working with Professor Marcos Dantus on femtosecond pulse shaping and its use in chemical identification and controlling laser matter interactions.

D. Ahmasi Harris received his B.S. in Physics and B.S. in Mathematics from Morehouse College in 1998. He received his M.S. in Optical Engineering and a Ph.D. in Applied Physics from the University of Michigan in 2002 and 2006, respectively. He is currently a postdoctoral associate with Professor Marcos Dantus, where his work focuses on laser control of molecular systems, laser−matter interactions, and novel applications of ultrafast spectroscopy.

Janelle C. Shane joined the Dantus research group in 2004 as an undergraduate researcher, where her research topics included search spaces of laser control problems. She received her B.S. in Electrical Engineering from Michigan State University in 2007 and is currently studying Physics at the University of St. Andrews as a National Science Foundation Graduate Research Fellow.

Marcos Dantus received B.A. and M.A. degrees from Brandeis University and a Ph.D. degree in Chemistry from Caltech. Under the direction of Professor Ahmed H. Zewail, he worked on the development of femtosecond transition-state spectroscopy, and as a postdoc, he worked on the development of ultrafast electron diffraction. He is presently a University Distinguished Professor in the Department of Chemistry and an Adjunct Professor in Physics at Michigan State University. Dantus has received many honors and awards. He is a Founder of KTM Industries and BioPhotonic Solutions, Inc. Professor Dantus's teaching interests include enhancing critical thinking in the classroom through activities involving discovery, student presentations, and competition-based games. One of his favorite challenges is teaching freshman students about what is NOT known in Chemistry. Professor Dantus's research interests include ultrafast dynamics, coherent laser control of chemical reactions, and biomedical imaging. Professor Dantus has over 120 publications and 13 patents and patent applications.

Χάος (Chaos), Κρονος (Chronos), and Αιθήρ (Ether) are discussed. The dream of controlling photochemical reactions using lasers and their ability to induce multiphoton excitation was first seriously discussed by Rousseau in 1966.[1] The main obstacle to implementing selective dissociation using long laser pulses is the fast intramolecular vibrational redistribution of energy (IVR). In 1980, Ahmed Zewail proposed using femtosecond laser pulses to overcome this obstacle.[2] The study of chemical reaction dynamics with femtosecond pulses, an endeavor now recognized as Femtochemistry,[3−5] led to the observation of coherent motion in the transition state as the molecule proceeds to the product state. Optimization of the laser fields to control chemical reactions was proposed by Tannor and Rice,[6] while Brumer and Shapiro realized that coherent light from the laser would allow them to cause interference between particular photochemical pathways, opening an attractive means for laser control of chemistry with nanosecond lasers.[7] The concept of creating a molecular wave packet that could be followed in time to cause selective chemistry by two or more carefully timed pulses was outlined by Rice, Kosloff, and Tannor.[8] By the 1990s, scientists began to modify femtosecond laser pulses by adding linear chirp, first to control wave packet motion[9] and then to control the yield of chemical reactions.[10]

The continued interest in laser control of chemical reactions is reflected by the high number of publications in peer-reviewed journals, which exceeds 30 articles per year. Several review articles of this large body of work are available: theoretical and experimental efforts toward wave packet control from 1926 to 1996 are summarized in a comprehensive review by Manz.[11] The experimental work on adaptive quantum control was reviewed by Brixner and Gerber in 2003.[12] Our group published a comprehensive review of modern (1997−2005) experimental results on coherent laser control of physicochemical processes.[13] The combination of shaped femtosecond pulses with mass spectrometry (MS) has been hailed as the most promising technology for laser control of chemical reactions. However, despite all of the high hopes, there are only a handful of groups across the world that have conducted these types of experiments. The pioneers in this field are Gustav Gerber, who published a series of papers beginning in 1998,[14−18] Robert Levis and Hershel Rabitz beginning in 2001,[19−21] Ludger Wöste beginning in 2001,[22,23] Thomas Weinacht starting in 2004,[24−29] and Robert Jones in 2005.[30] All of their experiments are based on a closed-loop approach using learning algorithms to control the laser fields with feedback from the experimental signal.[31] Our group has followed a different approach, often called open-loop, in which sets of different shaped pulses are evaluated for their ability to control chemistry.[32−36] There have been two articles that compare closed- and open-loop approaches to control the fragmentation of S_8[30] and ethanol.[37] Control of fragmentation with chirped pulses was published a few years ago.[38,39] To date, the laser-controlled fragmentation of the following molecules has been studied: S_8,[30] CH_4,[39] C_6H_{12},[40] C_7H_{14},[40] C_8H_{10},[40] C_2H_6O,[37,38] $C_2H_7O_3$,[32] $C_3H_6O_3$,[18] C_4H_6O,[19] C_8H_8O,[19,21,41] $C_8H_{10}O$,[41] C_5H_5N,[32] $C_8H_{11}N$,[41] C_5O_5F,[14,15,17] $C_3H_3OD_3$,[26] CH_2ClBr,[16] CH_2BrI,[26] $C_3H_3OF_3$,[19,24−27,29] $C_3H_3OCl_3$,[24,26] $C_3HBr_2OF_3$,[28] $C_7H_5FeO_2Cl$,[14−17] $C_7H_5FeO_2Br$,[17] $C_5H_5FeO_2I$,[17] and $C_7H_7NO_2$.[33,35,40]

For all of the molecules that have been studied, the absolute yield of the molecular ion is always maximized when transform-limited (TL) pulses are used. This universal observation has a simple explanation: when the pulses are shorter than 100 fs, the strong off-resonance field plucks out an electron from the molecule, yielding the molecular ion, a process known as field ionization. Another general result, gleaned from a number of published projects, is that the relative yield of heavy fragments to lighter fragments is maximized for TL pulses and minimized for longer pulses. This observation can be confirmed, for example, by consulting the work from Kosmidis and Ledingham on nitrotoluene[42−45] or from our group on *para*-nitrotoluene.[33] There are a few exceptions to this rule, for example, benzene, acetone, and tricarbonyl-[η5-1-methyl-2,4-cyclopentadien-1-yl]-manganese, which are shown in this article.

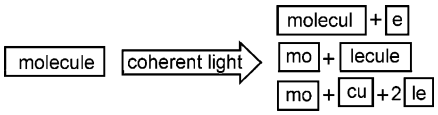

Figure 1. Cartoon illustrating different pathways for coherent laser control of a chemical reaction. The yield of each product depends on the time−frequency profile of the laser pulse.

The goal of laser control in the context of this article is to increase the yield of a desired fragment ion while suppressing the yield of other undesired fragment ions. This goal is illustrated by a simple cartoon in Figure 1. One can assess "selectivity" simply by obtaining the ratio between the intensity of two fragment ion lines in a mass spectrum. On the basis of the previous observations, the experiment could be trivialized by simply making the pulse as short or as long as possible to observe the greatest change in the aforementioned ratio. By phase modulation, one can stretch the pulse from tens of femtoseconds to tens of picoseconds. If, as discussed above, the greatest control is achieved for near-TL or maximally stretched pulses, then linear chirp ought to provide a simple one-parameter approach to optimization. Beyond this relatively obvious conclusion, we look for evidence of a type of shaped pulse that is capable of introducing energy into the molecule in such a way that arbitrary selective bond fragmentation is caused. We experimentally search for the elusive pulse among hundreds-of-thousands of shaped pulses following a number of strategies inspired by physics, spectroscopy, and reaction dynamics. We search for evidence of selectivity not only between two discrete product ions but within the entire mass spectrum. The guiding question for our work is, how do different phase modulation strategies affect molecular fragmentation? The informal working title of this research was "Everything you always wanted to know about laser control of molecular fragmentation but were afraid to ask", a rephrase of the title of the best-seller by David Reuben and famous movie by Woody Allen.

This article presents a comprehensive and systematic search for selective fragmentation of *para*-nitrotoluene (*p*-NT), analyzed using time-of-flight mass spectrometry (TOF-MS). We chose *p*-NT as an example of a medium-sized molecule with known spectroscopy; additionally, the functionalized aromatic ring gives *p*-NT relative structural complexity. Furthermore, this molecule has been used to refine explosives detection. The mass spectrum of *p*-NT measured with 70 eV electron impact[46] is presented in Figure 2a, with the molecular ion at *m*/*z* 137. The absorption spectrum[46] is presented in Figure 2b, and the excited states S_2 and S_3 are identified based on the literature.[47] The ionization energy (IE) and appearance energy (AE) of many ionic fragments have been measured with synchrotron radiation[48] and are presented in Figure 2b. As seen in Figure 2b, at least 3 photons are required for excitation of the lowest singlet state, 6 photons for the ionization of the parent ion, and 7−10 photons to access the different fragmentation pathways leading to ionic products.

The presentation is organized as follows. In section II, we give a detailed description of the experimental setup, including

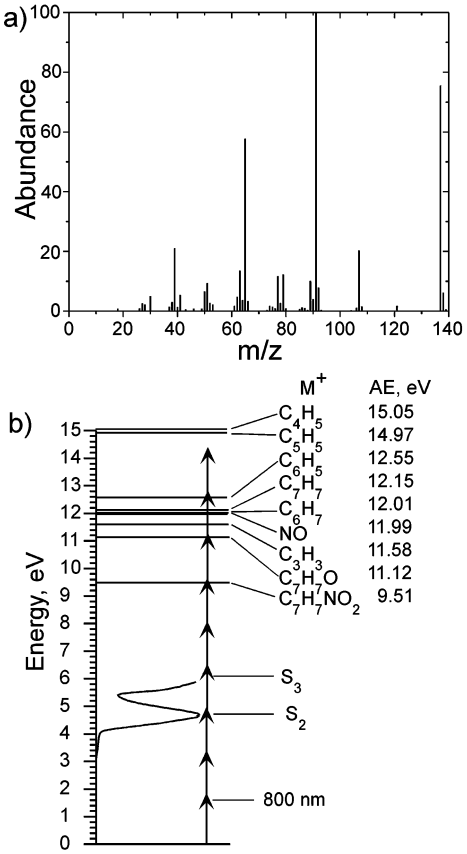

Figure 2. a) Mass spectrum of *p*-NT at 70 eV electron impact ionization. b) Optical absorption spectra and appearance energies of main fragmentation products by optical synchrotron excitation of *p*-NT.

examples of different shaped pulses, analysis of the laser-irradiated volume, and the effect of power and spot size of the beam on the mass spectrum. In section III, experimental results on *p*-NT, including intensity, pulse duration, and wavelength for TL pulses, effects of quadratic phase modulation (chirp) along with period and phase modulation of a sinusoidal phase function, and effects of binary phase, amplitude, and phase−amplitude modulation, are presented. The dependence of the fragmentation patterns on energy density is explored. Statistics of the total yield and selectivity of fragmentation for experiments using binary phase modulation are analyzed. Our findings for *p*-NT are tested for universality by carrying out experiments on 16 other molecules. Fragmentation patterns are found to vary monotonically with respect to the total yield of ions regardless of phase modulation. Finally, intensity and volume effects are measured, and their influence on our findings is reported. The results are discussed in section IV starting with a discussion on the fragmentation mechanism for *p*-NT. The general trends uncovered by our study for all of the different molecules are summarized. The advantages of a systematic approach to laser control are discussed and compared to closed-loop experiments. Finally, we illustrate a reaction pathway that is highly sensitive to the type of phase modulation and deviates from the general trends observed for the rest of the pathways. In section V, conclusions are drawn from all of the data gathered for all of the molecules studied here.

II. Experimental Methods

1. Laser System and Pulse Shapers. A schematic of our laser system is presented in Figure 3. The Ti:Sapphire oscillator (K&M Labs) is pumped by the second harmonic of a Nd:YVO_4 laser (Spectra-Physics, Millennia), resulting in femtosecond

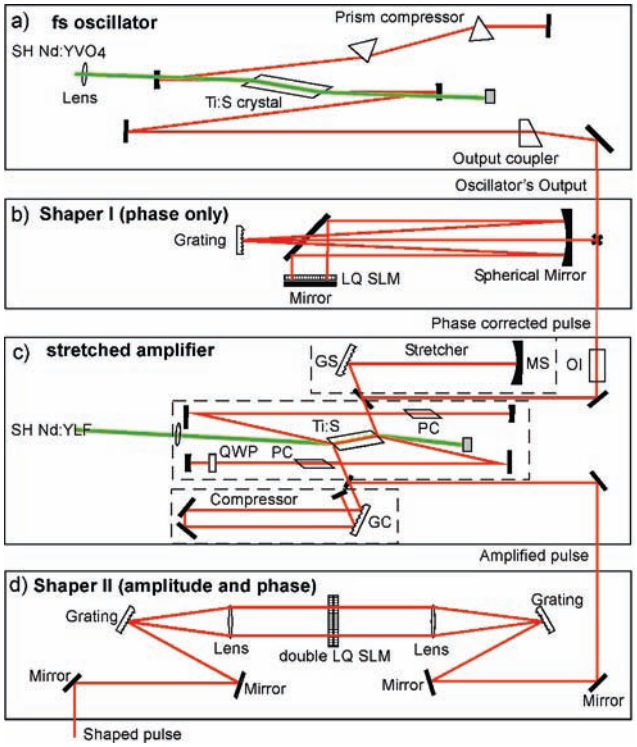

Figure 3. Schematic of the laser system including a) a fs laser oscillator, b) a folded phase-only pulse shaper, c) a regenerative laser amplifier, and d) a phase and amplitude pulse shaper.

pulses with a center wavelength of 800 nm and a spectral bandwidth of 40 nm fwhm at 80 MHz and an average power of 300 mW (see Figure 3a). The output from the oscillator is collimated with a telescope and is directed to the first pulse shaper (pulse shaper I), located between the oscillator and the amplifier (see Figure 3b). Pulse shaper I has an 830 groves/mm dispersive grating, a 15 cm focal length spherical mirror, and a 128 pixel liquid crystal spatial light modulator (SLM-128, CRi) in a reflective mode. The spectral phase modulation applied by pulse shaper I is preserved during amplification, a fact that has been experimentally verified,[49] and was used for phase shaping experiments to systematically apply predetermined pulse shaping strategies.

The amplifier used in this system (see Figure 3c) is a Ti:Sapphire regenerative amplifier (Spectra-Physics, Spitfire) pumped by the second harmonic of the Nd:YLF laser (Spectra-Physics, Evolution X, 1 kHz), which gives 800 nm pulses at 1 kHz with an energy of about 800 μJ. The bandwidth of the output pulses is ~30 nm fwhm, which results in 35 fs (fwhm) transform-limited pulses.

The shaped output of the amplifier is used for experiments that require phase-only pulse shaping. Pulse shaper II is used for experiments that require amplitude and phase pulse shaping. Pulse shaper II consists of two identical dispersive gratings (830 groves/mm), two identical cylindrical lenses (F = 225 mm), and a dual-mask 128 pixel liquid crystal SLM (SLM-256, CRi) programmed for applying both amplitude and phase shaping. The setup is arranged in an unfolded 4f geometry (see Figure 3d). The spectral resolution of the two pulse shapers is ~1 nm/pixel. Pulse-to-pulse variation in the energy of the pulses for the amplified system is 2%. The spectrum of the second-harmonic generation (SHG) of the shaped laser pulses is measured after frequency doubling in a 50 μm type-I β-BBO crystal using a miniature spectrometer (USB2000 Ocean Optics) and

is used to establish pulse shaping reproducibility. The pulse-to-pulse variations in the measured SHG signal were less than 4%.

Before each set of experiments, the beam is characterized at the sample, and spectral phase distortions are corrected using multiphoton intrapulse interference phase scan (MIIPS),[50−52] with pulse shaper I. MIIPS is a method for spectral phase measurement and adaptive phase compensation, introduced in 2003, that is based on multiphoton intrapulse interference.[53,54] Unlike methods based on autocorrelation or interferometry, MIIPS uses a pulse shaper to introduce a series of calibrated reference phase functions that cause a cancellation of the local chirp (second derivative of the spectral phase). At those frequencies the SHG spectrum exhibits maximal intensity. The complete set of SHG spectra obtained for the different reference phases contains sufficient information to obtain the second derivative of the phase across the spectrum of the laser. Double integration yields the phase distortions. By setting the pulse shaper to the negative values of the measured phase distortion at each frequency, the phase distortions are eliminated.[50−52] Spectral phase distortions are corrected to less than 0.1 rad across the fwhm of the spectrum to obtain true TL pulses. For all experiments, we start with pulses having $\tau/\tau_{TL} = 1.001$, where τ and τ_{TL} are the calculated pulse durations with and without the measured residual phase distortions, respectively. A time delay between subsequent pulse shaping masks of 0.5 s is introduced to minimize relaxation effects that could occur in the liquid crystal in the SLM units; experimentally, we determine that after 0.1 s, the phase mask is stable.

2. Typical Shaped Pulses. Figure 4 shows some of the typical shaped pulses produced by our system. The left column shows the spectrum of the pulses (dashed line) centered around 800 nm, along with the phase functions applied to the pulses (solid line). The right column shows the calculated effect of the phase modulation on the pulses in the time domain. Each row displays the effects of the different kinds of pulse shaping used in our experiments. The shaped pulses shown have a second harmonic spectrum whose integrated intensity is 25% of that of transform-limited pulses.

The amplitude of the complex fundamental spectrum is the square root of the measured power spectrum in the frequency domain $I(\omega)$ and the phase $\phi(\omega)$ introduced by the pulse shaper. The complex spectrum of the electric field is given by

$$E(\omega) = \sqrt{I(\omega)}\,\exp[i\phi(\omega)] \quad (1)$$

To calculate the field in the time domain, we take the inverse Fourier transform of the complex fundamental spectrum

$$E(t) = \int E(\omega)\,\exp[-i\omega t]d\omega \quad (2)$$

Figure 4a shows the experimentally measured spectrum (left, dashed line) and the phase used for shaping it. Figure 4b shows the calculated time profile of our TL pulses with a 30 nm fwhm (right, dashed line) and the resulting intensity of the modulated pulses $I(t) = |E(t)|$.[2] Figure 4 panels b and c show the effect of applying positive and negative quadratic chirp to a TL pulse. Formally, we write the phase function for quadratic chirp as $\phi(\omega) = 0.5\phi''(\omega - \omega_0)^2$, with ϕ'' in units of fs^2. Applying chirp to a Gaussian pulse yields a time profile that is still Gaussian but stretched out in time and therefore reduced in intensity. The slight deviation from a Gaussian time profile shown here results from the fact that our experimental spectral profile was not perfectly Gaussian. In Figure 4b, $\phi'' = 2500$ fs^2, while in Figure 4c, $\phi'' = -2500$ fs^2.

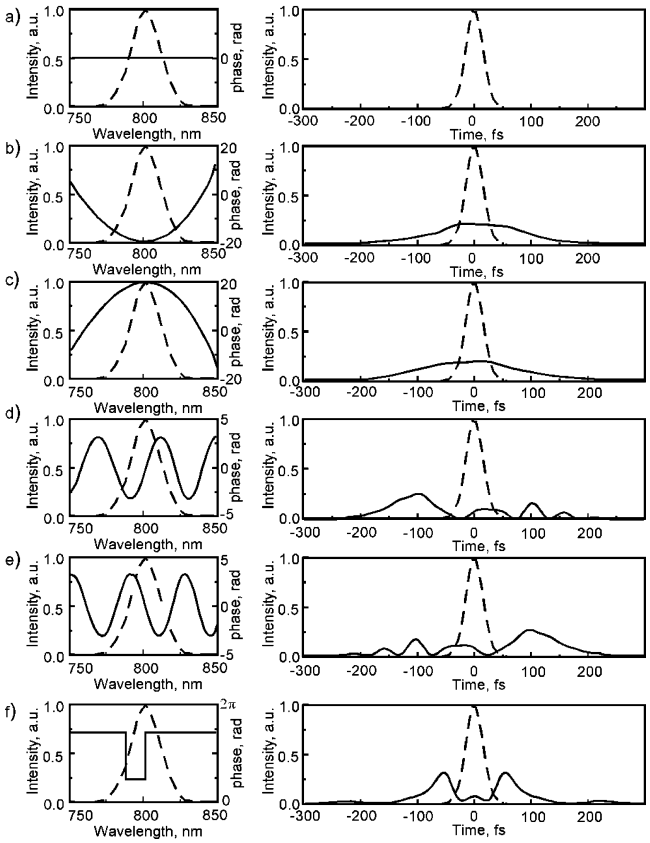

Figure 4. Typical field shapes of phase-modulated femtosecond laser pulses. Left column: spectral power (dashed line) and phase (solid line); right column: calculated time profile of the intensity. a) Phase compensated TL pulse (dashed line), the starting point for the generation of shaped laser pulses. b) and c) Positively and negatively chirped pulses with sinusoidal phase function $\phi = \pm 2500\text{fs}^2(\omega - \omega_0)^2/2$. d) and e) Laser pulse with sinusoidal phase function $\phi = \pm\pi \sin[35\text{ fs}\ (\omega - \omega_0)]$. f) Binary phase modulation, where the phase is evenly modulated in the frequency domain with the string $\pi\pi\pi\pi00\pi\pi$.

Figure 4 panels d and e show the effect of sinusoidal phase modulation, where we varied the period γ, or the phase shift δ, according to $\phi(\omega) = \alpha \sin[\gamma(\omega - \omega_0) - \delta]$. Applying sinusoidal phase modulation causes the time profile of the pulse to spread, as well as to deviate from TL. In the examples shown, phase modulation produces a series of pulses of either decreasing amplitude (Figure 4d, where $\alpha = \pi$, $\gamma = 35$ fs, and $\delta = 0$) or increasing amplitude (Figure 4e, where $\alpha = \pi$, $\gamma = -35$ fs, and $\delta = 0$). Figure 4f shows an example of the effect of binary phase shaping. In binary phase shaping, the spectral phase is only allowed to take a value of 0 rad (assigned a value of "0") or π rad (assigned a value of "1") at discrete blocks of frequencies within the pulse spectrum. The phase function can then be represented as a binary string of 0's and 1's. This representation is similar to that used in areas of signal processing and mathematics for related problems. Binary phase functions can produce a variety of time profiles, but these time profiles will always be symmetric about $t = 0$. In general, the more the phase switches between 1 and 0, the more the time profile will be stretched, and the peak intensity will be reduced. The binary phase function shown in Figure 4f can be represented by the 8-bit string 11001111.

The different phase functions were chosen because each type controls a different plausible mechanism that could influence different photofragmentation pathways and cause selective bond cleavage. Chirped pulses cause a linear delay between high and low frequencies within the bandwidth of the laser pulses. This

temporal progression has been linked to pump−dump processes in the excitation of a laser dye in solution.[55] Sinusoidal modulation causes trains of pulses. Varying the time delay between these pulses, by varying the modulation frequency, may coherently drive vibrations that again could be implicated in selective bond cleavage. These resonant frequencies have been implicated in control experiments.[56] Changing the frequency where a single sinusoidal phase modulation crosses zero can be used to control the range of frequencies at which multiphoton excitation can take place. This type of phase modulation has been used to control two and three photon excitation in atoms[57] and in large molecules in solution.[53,54,58] Finally, we used binary phases because of their ability to control the amplitude of multiphoton excitations and to control selective stimulated Raman transitions.[59−61]

3. The Time-of-Flight Mass Spectrometer. A schematic of the TOF mass spectrometer is shown in Figure 5. The mass spectrometer has a linear geometry with a 0.5 meter field-free drift region. A base pressure of 10^{-7} Torr is maintained by a three-stage differential pumping scheme with a mechanical roughing pump, a diffusion pump, and a turbo pump. Experimental samples of *para*-nitrotoluene (*p*-NT, Aldrich 99%), *meta*-nitrotoluene (*m*-NT, Aldrich 99%), *ortho*-nitrotoluene (*o*-NT, Aldrich 99+%), 1-methyl-2,4-dinitrobenzene (DNT, Aldrich 97%), benzene (Aldrich 99+%), toluene (J T Baker 100%), naphthalene (Aldrich 99.7%), azulene (Aldrich 99%), acetone (Mallinckrodt 99.8%), acetyl chloride (Aldrich 99+%), acetophenone (Fluka >99.5%), *p*-chrolobenzonitrile (Aldrich 99%), *N*,*N*-dimethylformamide (DMF, Spectrum Chemicals 99.8%a), dimethyl phosphate (DMP, Aldrich 98%), 2-chloroethyl ethyl sulfide (h-MG, Aldrich 98%), and tricarbonyl-[(1,2,3,4,5-η5)-1-methyl-2,4-cyclopentadien-1-yl]-manganese (MMT, Aldrich 99.5%) were used without further purification. The sample is allowed to effuse into the chamber by an inlet valve up to a pressure of 10^{-5} Torr during experimentation. The pressure is an equilibrium reached by the vapor of the sample (cooled by an ice bath) and the fast pumping speed of a 4 in. turbomolecular vacuum pump. This ensures very fast flow and prevents the accumulation of photoproducts in the chamber. When the sample valve is closed, all ion signals disappear in less than 1 s, and the pressure drops to 10^{-7} Torr. The sample molecules are ionized by the laser beam and focused by a lens at the entrance of the time-of-flight chamber. The focusing lens is also used as the window of the chamber to minimize self-focusing effects that could appear if an external lens were used, as distortions of the light field by phase modulation have been found to affect MS measurements.[62,63] The polarization of the laser is horizontal as it enters the mass spectrometer and perpendicular to the ion collection optics. We attenuate the beam to 170 μJ/pulse unless otherwise noted, and no phase distortions due to the self-focusing are observed. The repeller plate is maintained at 2.5 kV. The extraction plate is 1 cm away from the repeller plate and is maintained at 1.6 kV, with a 5/8 in. diameter circular wire grid. For some experiments, we replace the extraction plate by a blank plate with a 0.7 mm diameter extraction pinhole. We find that the pinhole leads to a three-fold loss of signal, but no difference is found in the fragmentation patterns observed for TL or shaped pulses. The loss of signal may be caused by the horizontal recoil of the fragment ions. Unless noted, the experimental results presented here were obtained with an extraction grid. In order to examine volume effects, expected at higher intensities, we used an extraction plate with a 0.9 mm slit perpendicular to the laser beam. These measurements are presented in section IV. The

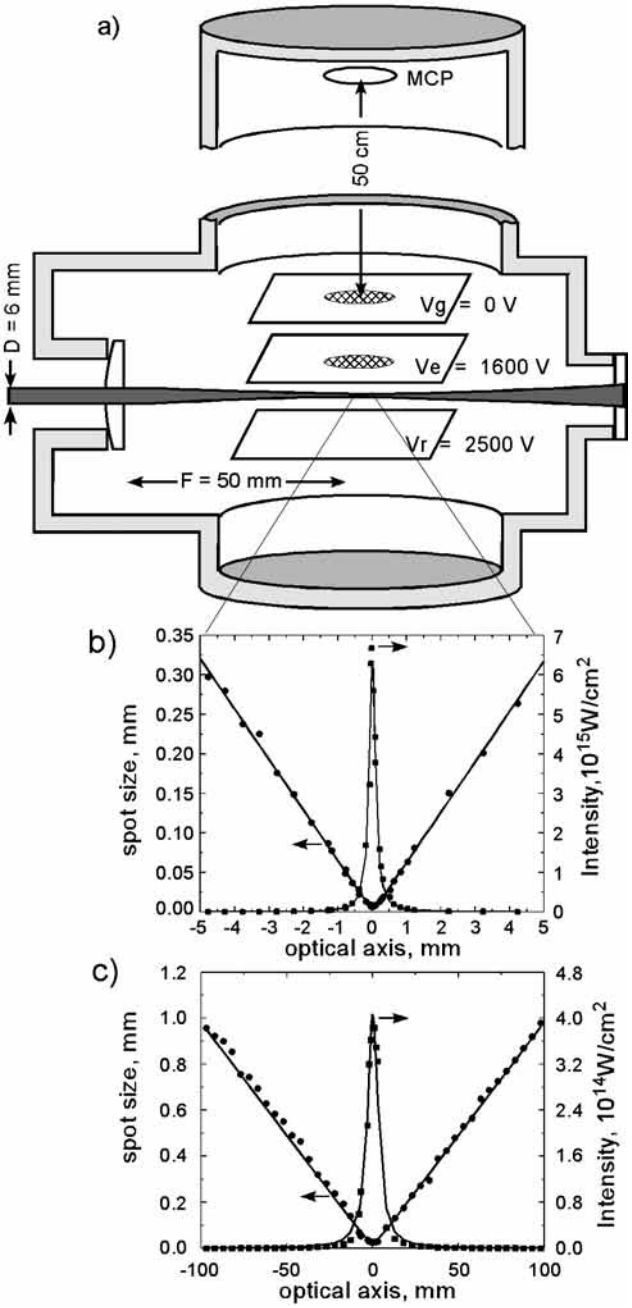

Figure 5. a) A schematic of the time-of-flight mass spectrometer. The laser beam is introduced into the chamber through a lens to minimize phase distortion. Ions, generated between the repeller/extractor pair at high voltage, accelerate to the flight tube, where they are registered by the dual microchannel plate detector. b) Graph showing the measured spot sizes of the beam waist along the optical axis of the laser for the 50 mm focal length lens with a Rayleigh length of 66 μm, together with the calculated peak power for 170 μJ TL pulses. c) Graph showing the same as that in b) but for the 300 mm focal length lens with a Rayleigh length of 2.2 mm.

extracted molecular ions pass through the extraction grid into the acceleration region. The ions are detected using a microchannel plate (MCP) detector coupled to a 500 MHz digital oscilloscope (Infiniium 54820A, HP). The MCP sensitivity has minimal *m*/*z* dependence[64,65] at our conditions, and was not taken into account. The unit mass resolution of our TOF system is approximately 250.

Two different focusing conditions were used for our experiments. For the highest intensities, we used a 50 mm focal length lens. For lower intensities and to explore the influence of volume

effects, a 300 mm focal length lens was used. The spatial profile of the beam was measured using a beam profiler (Coherent). The beam profile can be approximated to a Gaussian function, and the beam propagation ratio (M^2) was found to be 1.04 and 1.5 for the 300 and 50 mm lenses. The spot size of the beam was measured by scanning a blade across the beam. The minimum spot size ω_0 (radius where the intensity decreases by $1/e^2$) was 6.4 and 25.9 μm for the 50 and 300 mm lenses, respectively. The spot size of the beam increases away from its minimum value with a Rayleigh range (z_R) of 66 μm and 2.2 mm for the 50 and 300 mm lenses. The spot size dependence along the optical axis is shown in Figure 5b and c for both focusing lenses, together with the prediction for the Gaussian beam (line). The maximum intensities I_0 of the beam were calculated with the formula $I_0 = 4(\ln(2))^{0.5}\,\pi^{-1.5} \times W \times \tau^{-1} \times \omega_0{}^{-2}$, where W is the energy of the pulse (J), τ is the duration (fwhm) of the pulse, and ω_0 is spot size. The calculated dependence of the maximum field intensity along the optical axis is shown in Figure 5b and c together with a simulation (Lorentzian line shape). In order to check the accuracy of our intensity measurements, we measured the ionization threshold for He atoms using the 50 mm focal length lens. The obtained value (1287×10^{12} W/cm^2) is in good agreement with the value (1158×10^{12} W/cm^2) reported by Hankin et al.[66]

According to modern theories, the threshold for molecular ionization (I_s) is between 1.0×10^{14} and 1.5×10^{15} W/cm^2.[67] The peak field intensity (I_f) for the 35 fs TL pulse at the focal region, shown in Figure 5b, is 7×10^{15} W/cm^2. The volume of the sample (V_i) above ionization threshold (I_i) calculated using the formula from the review in ref 68 is $V_i = 2/9\pi\omega_0{}^2 z_R (I_f/I_i)^{3/2}$. At 10^{-5} Torr pressure, the calculated volume $V_i \sim 10^{-8}$ cm^3 results in 10^5 molecules being ionized. Approximately 75% of the ions from this volume are detected by the TOF mass spectrometer. We collected mass spectra in the range of pressures from 10^{-6} up to 2.2 10^{-5} Torr and found no change in the relative yields of ions with pressure although the combination of very high laser intensity and very high sample pressure resulted in space−charge broadening of some peaks. This condition was avoided in the experiments presented here.

The raw mass spectrum of *p*-NT obtained with 6×10^{15} W/cm^2 TL pulses is presented and the main fragment ions are labeled in Figure 6a. After identification of several "fingerprint" ions in the raw MS spectrum, we can transform the ion drift time to a *m*/*z* scale. Mass spectra obtained for TL 6×10^{14} and 1×10^{13} W/cm^2 are shown in Figure 6b and c, respectively.

A bar diagram is calculated from integrals under the corresponding peaks in the MS data. Because pulse shaping affects the MS, we present our results as a percentage of total ionization (*Y*, %).[69] Standard deviations in the bar graph (see Figure 7a) are small and were calculated using 6−10 repetitions of the experiments. In Figure 7, we demonstrate MS following excitation with a TL pulse and for pulses stretched up to 635 fs by a quadratic phase modulation of $\phi'' = \pm 8000$ fs^2 introduced by shaper I. As we can immediately see from Figure 7, the shape of the MS spectra is different for TL and chirped pulses and does not depend on the sign of the phase modulation. To assess selectivity, we primarily point to the intensity of fragment ions with *m*/*z* 91 and 39 (see Figure 7). Although this is only one of several different ratios we could report, we discuss control over all of the different fragment ions in the later sections of this article. In section IV, we comment on changes observed on minor product pathways, for example, on NO_2^+ with *m*/*z* 46, which does depend on the sign of the chirp and reaches its maximum yield near $\phi'' = -8000$ fs^2.

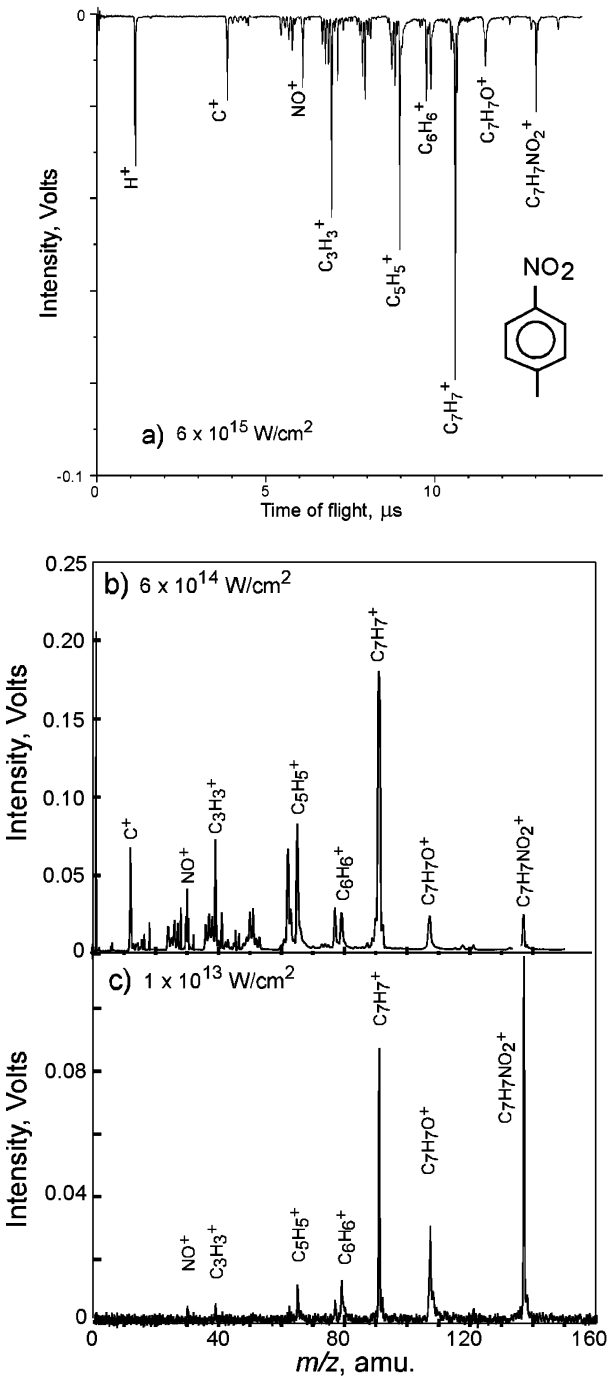

Figure 6. Mass spectra for *p*-NT obtained for TL pulses. (a) Oscilloscope trace of the time-of-flight mass spectrum for 6×10^{15} W/cm^2. Mass spectra obtained for 6×10^{14} (b) and 1×10^{13} W/cm^2 (c). Absolute voltage values depend on the number of amplification stages.

4. Effect of Focusing. MS results can be influenced by the focusing parameters.[68,70,71] We wanted to make sure that the results that we obtained are general and can be used to explain experiments carried out elsewhere. Therefore, we explored how changes in the focusing parameters affect the observed results.

Laser intensity dependence measurements were carried out on *p*-NT using both short and long focusing geometries. The measurements with the longer focal length were made using a slit to limit the *z*-axis contribution to the volume effect.[66,72,73] From the measurements presented in Figure 8a, we find the expected initial rise of the signal and its change to a linear dependence as the power increased. From these data, we obtain

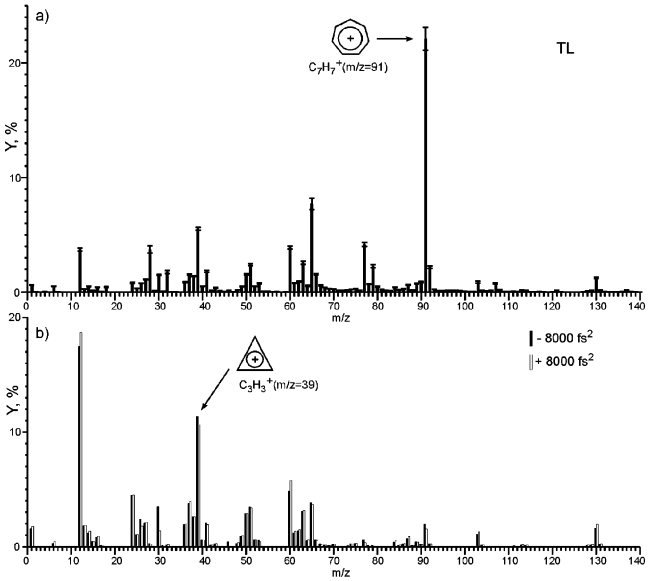

Figure 7. Bar diagrams of the mass spectra of *p*-NT. a) Percentage of the total ionization for each *m*/*z* value at TL excitation; standard deviations of these measurements are marked as error bars. b) Mass spectra using positively and negatively chirped pulses. The two most abundant molecular products, which are used for selectivity analysis, are identified in the spectra.

a value for the I_{sat} of 1.7×10^{14} W/cm^2, which is in the range of expected values for organic molecules. The interpretation of I_{sat} has been discussed in detail by Corkum.[66,72] In the simplest approximation (sudden model), I_{sat} is assumed to indicate a value where 100% of the species in the focal volume are ionized. In the case of multiphoton ionization, I_{sat} is defined as the intensity at which 43% of the molecules in the laser-irradiated volume are ionized.[66,72] Obviously, above I_{sat}, one can expect high signal-to-noise ratios because signals are quite robust. At values below I_{sat}, pulse shaping causes a significant drop in the signal, greatly reducing the reliability of the measurements. Most of the experiments presented here were carried out above I_{sat} under the conditions shown in Figure 6b, without the extraction plate slit. If laser-controlled chemistry will have a practical application, it is only above I_{sat} that a significant yield of products could be achieved. A discussion and experimental evaluation of our findings near and below I_{sat}, including a quantitative analysis of volume effects is given in Section III.11

Having chosen the shorter focal length arrangement, we explored effects caused by changing the diameter of the beam before the focusing lens while adjusting the power of the laser to keep the energy of the pulse constant. These measurements probe the effect of changes in the Rayleigh length of the beam on our findings. We observed that the MS yield increased as the input beam diameter decreased (see Figure 9a). This observation can be explained by realizing that decreasing the diameter of the input beam causes an increase in the spot size and Rayleigh length. These increases cause the irradiated volume, where the field strength exceeds the threshold for ionization, to increase. Therefore, more molecules can be ionized. It is important to note that the ratio between the fragment ions with *m*/*z* 91 and 39, and in general the overall shape of the mass spectrum, was found to be independent of the diameter of the laser beam or the average laser power (Figure 9b). Therefore, we conclude that although focusing parameters can change the overall signal level and the volume from which the ions are generated, these changes do not influence the ability of the laser parameters to change the fragmentation pattern which we are using here as a measure for selectivity. The changes observed as a function of intensity for both short and long focusing conditions are discussed in Section III.11.

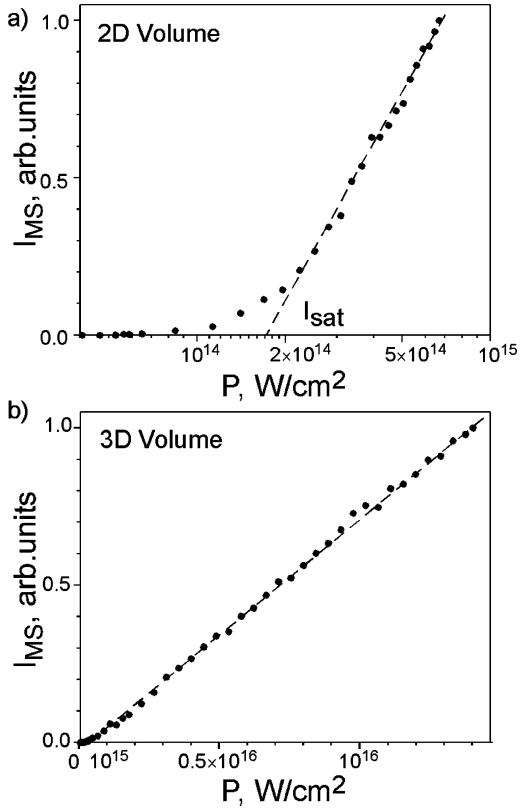

Figure 8. Power dependence of the total yield of ionization of *p*-NT. a) Experiment carried out using the 300 mm focal length lens and a 0.9 mm slit on the extraction plate. b) Experiment carried out using a 50 mm focal length lens with a wire grid extraction plate.

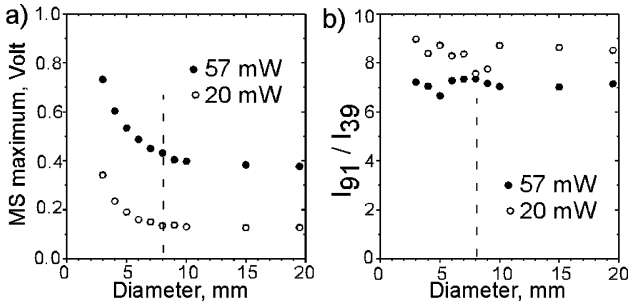

Figure 9. a) Dependence of strongest line (*m*/*z* 91) total TOF MS yield on the diameter of the iris used to cut the beam, shown at two different laser powers. The dashed line is the beam waist size of the collimated beam used in all subsequent experiments. b) Ratio between integrated MS signals from two products at different powers and beam diameters.

III. Results

1. Effects of Power, Bandwidth, and Carrier Frequency of TL Pulses. Our first set of experiments explored the effect of power, pulse duration, and carrier frequency for TL pulses on the fragmentation and ionization of *p*-NT. The power of the pulse was changed using a zeroth-order half-wave retardation plate and a calcite polarizer. The pulse duration and carrier frequency changes were achieved using amplitude modulation in shaper II. The group velocity dispersion on the pulse for each setting was compensated for each measurement using MIIPS.[50−52] The results of these experiments are collected in Figure 10. Column I shows the dependence of the integrated SHG obtained after a frequency-doubling crystal (I_{SHG}) and is used as a

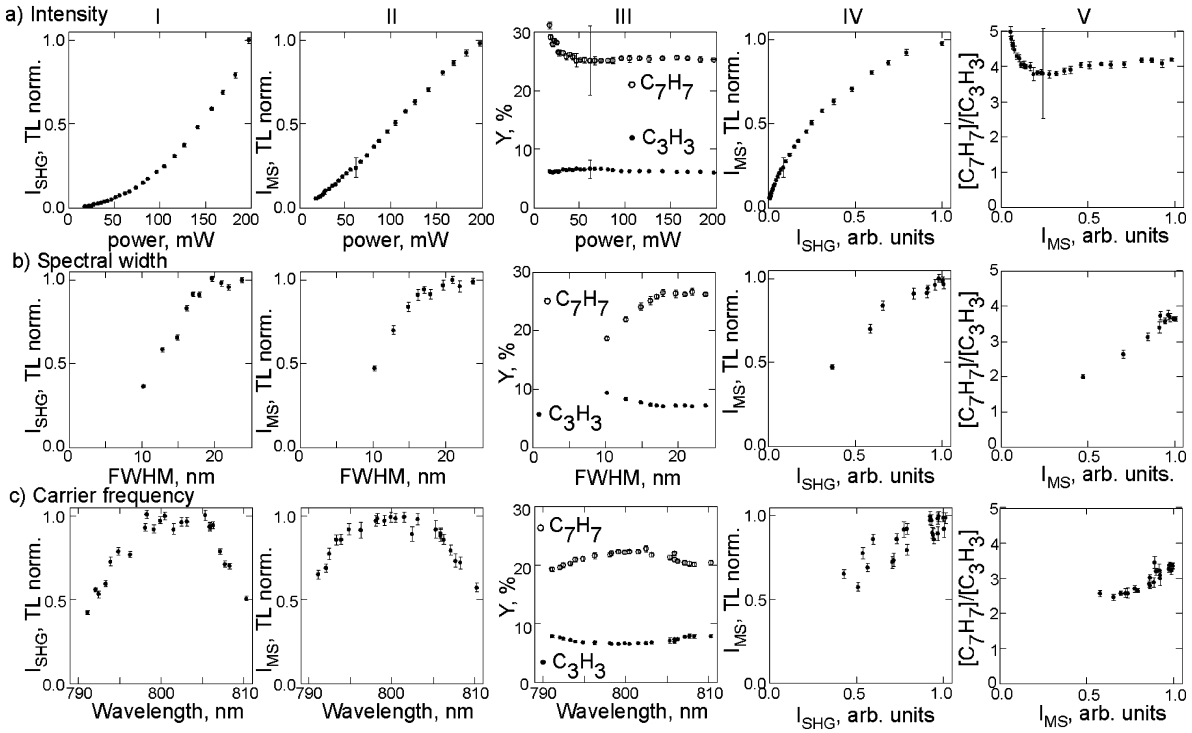

Figure 10. Experimental fragmentation results with a) different pulse energies but constant 35 fs duration, b) different spectral widths at a constant 50 mW laser energy, and c) different carrier frequencies at a constant 35 fs pulse duration and 50 mW laser energy. The columns denote (I) the dependence of the energy of the SH generated in the nonlinear crystal, (II) the dependence of the total yield of all positively charged ions, (III) the yield (percentage of total ionization) of two major fragments, (IV) the total yield of all fragments as a function of the intensity of SHG in the crystal, and (V) the selectivity (ratio between fragments) as a function of total yield of all fragments. All results are given with the standard deviations of the measurements as error bars obtained from 10 runs, averaging 128 laser pulses each. Yields are normalized to the maximum value.

diagnostic, column II shows the integrated yield of all ions (I_{MS}), and column III shows the percentage of total ionization (Y,%) of two different fragment ions (C_7H_7 and C_3H_3) as functions of the scanned parameters. Column IV shows the integrated ion intensity (I_{MS}) plotted against the measured integrated SHG (I_{SHG}). Column V shows how the ratio between the yields of the two fragment ions (m/z 91 divided by m/z 39) depends on the integrated ion intensity. The intensities I_{SHG} and I_{MS} were normalized to the value measured for TL pulses. The first row (a) presents results as a function of average power (at constant spectral shape corresponding to 35 fs time duration); the second row (b) presents results as a function of the spectral width of the pulse while the intensity of the laser is held at 50 mW; The third row (c) presents results as a function of the position of the pulse maximum while the fwhm of the spectral width is restricted to 15−17 nm.

The results from the first row in Figure 10 show the expected quadratic dependence of the SHG intensity on the intensity of the laser. In this range, $10^{15}-10^{16}$ W/cm^2, the total ion intensity was found to increase linearly with the power of the pulse. Despite the order of magnitude change in laser intensity and the similarly large change in the excitation volume, the ratio between the two different fragment ions stays constant. The results in the second row show the dependence on bandwidth. We see that the total ion yield tracks with the integrated SHG signal, as confirmed by the nearly linear relationship between the two in column IV. The yield of the heavy and light ions changes as a function of bandwidth. The broader bandwidth (TL) pulses favor the larger ions. The results in the third row explore possible effects caused by the carrier frequency. Most importantly, the ratio between the two different fragment ions remains constant, indicating that selectivity is not a function of carrier frequency.

2. Effects of Quadratic and Sinusoidal Phase Modulation on SHG, Total Fragmentation Yield, and Selectivity. In the second set of experiments, we explored changes that are caused by phase-only modulation, with the laser spectrum kept constant. The experimental results are summarized in Figure 11. The average power of the beam was 170 mW at 1 kHz, and the pulse duration of the corresponding TL pulse was 35 fs. Column I shows I_{SHG}. Column II shows the total ionization yield I_{MS}. Column III shows relative yields of the two fragments. Column IV shows the relation between the total ionization yield and the intensity of the SHG. Column V shows the ratio of the two fragments as a function of total ionization yield. The results in the first row (a) show the effects caused by linear chirp, more precisely known as quadratic phase modulation (ϕ'') which is introduced by shaper I. We see that I_{MS} and I_{SHG} have a very similar dependence, which is confirmed in panel IV. We measured an overall laser control factor $R_{max}/R_{min} = ([C_7H_7]/[C_3H_3])_{max}/([C_7H_7]/[C_3H_3])_{min} = 30$, achieved here by simple chirp. Interestingly, we also observe that the light and heavy fragment yields have a linear relationship, as evidenced by panel V. The second row (b) shows the effects caused by changing the period of a sinusoidal phase modulation (γ, while keeping $\delta = 0$). We scanned positive as well as negative values in order to explore possible effects of the temporal symmetry of the pulse. For sinusoidal modulation, the temporal profile of the pulse changes depending on the sign; for example, see Figure 4d and e. Once again, we see that I_{MS} and I_{SHG} have a very similar dependence, which is confirmed in panel IV. We measured an overall laser control factor $R_{max}/R_{min} = 10$. We also see that the light and heavy fragment yields have a linear relationship, as evidenced by panel V. The slight asymmetry between positive and negative γ appears as a slight deviation in the linear relationship between I_{MS} and I_{SHG}. We think that

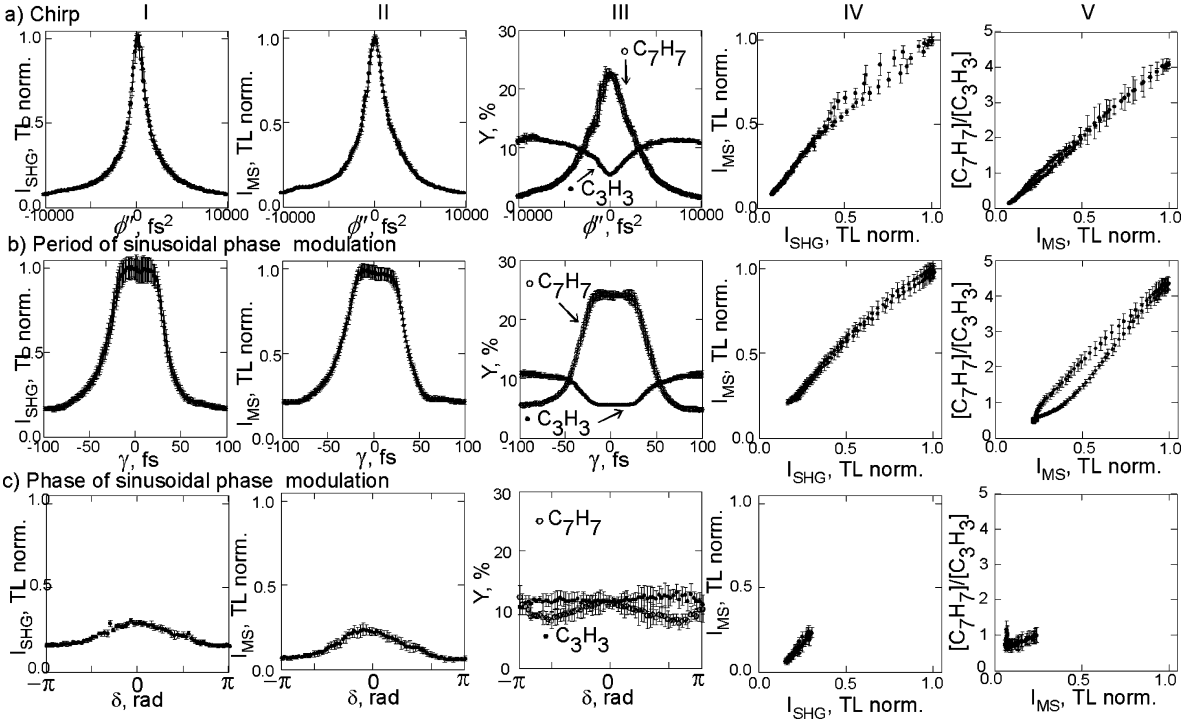

Figure 11. Experimental results on fragmentation using phase-only shaped femtosecond pulses with a) differing amounts of quadratic chirp ω, with phase functions given by $0.5\phi''(\omega - \omega_0)^2$, b) sinusoidal phase modulation with different periods γ, with phase functions $\pi \sin[\gamma(\omega - \omega_0)]$, and c) sinusoidal phase modulation with different phase delays δ, with phase functions $\pi \sin[35 \text{ fs } (\omega - \omega_0) + \delta]$. The columns denote (I) the dependence of the energy of the SH generated in the nonlinear crystal, (II) the dependence of the total yield of all positively charged ions, (III) the percentage of ionization of two main fragments, (IV) the total yield of fragments as a function of the intensity of SHG in the doubling crystal, and (V) the selectivity as a ratio between fragments as a function of the total yield of fragments. All results are given with the standard deviations of the measurements as error bars obtained from 10 runs, averaging 128 laser pulses each. Yields are normalized to the value obtained at TL excitation.

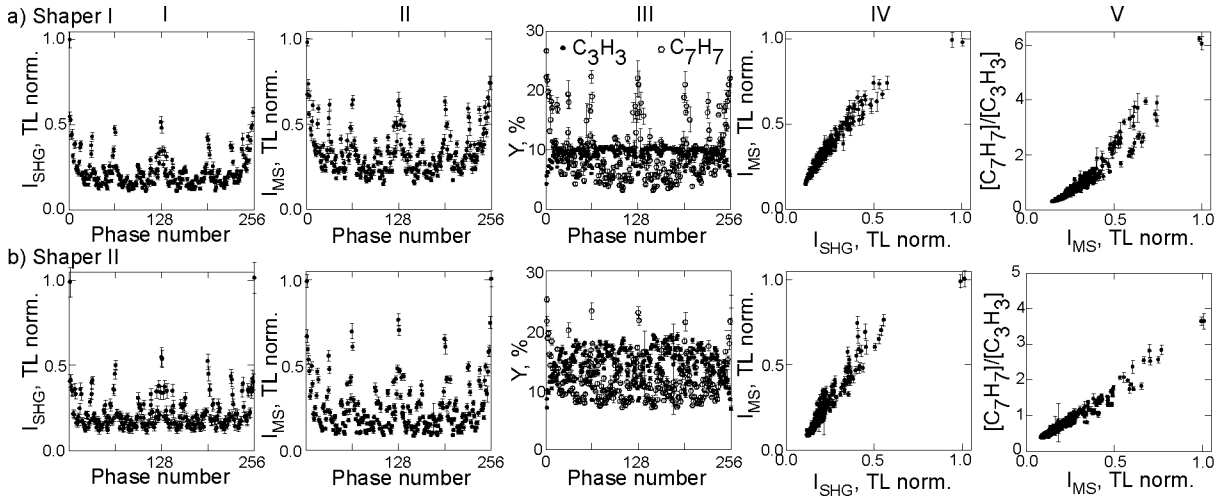

Figure 12. Experimental results on fragmentation using binary phase-modulated femtosecond pulses a) using a shaper between the oscillator and amplifier and b) using a shaper after the amplifier. The columns denote (I) the dependence of the energy of the SH generated in the nonlinear crystal; (II) the dependence of the total yield of all positively charged ions, (III) the percentage of ionization of two main fragments, (IV) the total yield of fragments as a function of the intensity of SHG in the doubling crystal, and (V) the selectivity as a ratio between fragments as a function of the total yield of fragments. All results are given with the standard deviations of the measurements as error bars obtained from 10 runs, averaging 128 laser pulses each. Yields are normalized to the value obtained at TL excitation.

this deviation is caused by an imperfection of the phase modulator, particularly the effect of phase wrapping[13] in the SLM after the distortion compensation and additional phase function are implemented. The third row (c) shows the effects caused as sinusoidal phase functions are introduced with different values for δ while keeping $\gamma = 35$ fs. We see that changing δ causes small changes in all of the observed variables compared to the other modes of phase modulation. Changes in δ cause changes in the frequencies at which multiphoton transitions can take place.[53,54] The modest laser control factor $R_{max}/R_{min} = 1.5$ observed here indicates that resonant multiphoton transitions play a minimal or no role in the fragmentation of this molecule under the conditions of our experiments.

3. Effects of the Binary Phase on SHG, Total Fragmentation Yield, and Selectivity. In the third set of experiments, we explored the effects caused by binary phase modulation using shaper I (before the amplifier) and shaper II (after the amplifier). For these experiments 8-bit functions were used. The central six logical bits correspond to groups of binned pixels in the central part of the spectrum (the region for which the spectral

intensity was greater than 25% of the maximum). The blue and red spectral wings of the pulse were assigned as the 0th and 7th bits of the 8-bit sequences, where logical 0 corresponds to a phase value of 0 rad and logical 1 corresponds to phase value of π rad. The average power of the beam was 100 mW, and the pulse duration of the corresponding TL pulse was 35 fs. The columns in Figure 12 follow the same arrangement as those in Figures 10 and 11. The results also confirm that phase modulation by shapers I and II is equivalent. Interestingly, once again we see that the measured I_{MS} and I_{SHG} have a linear dependence, which is confirmed in panel IV. The laser controllability factor R_{max}/R_{min} observed for 8-bit binary phase shaping was 20 for shaper I and 10 for shaper II. This difference may be caused by slight beam distortions caused by the limited height of the liquid crystal mask, which is smaller than the beam diameter and apertures of the beam.

4. Effect of Laser Pulse Energy Density. Experimental measurements with four different phase functions were repeated using four different laser pulse energies, ranging from 2×10^{15} to 1.5×10^{16} W/cm^2 when TL, in order to determine if molecular fragmentation depends on the laser pulse energy density. As we can see in Figure 13, the relative yield of C_7H_7 and C_3H_3 ions is independent of the energy of the pulse for all types of phase modulation. These results may seem to contradict results in the literature for which laser pulse intensity did change the relative yield of fragment ions. Given that a complete review of all such observations is beyond the scope of this article, we limit our explanation to our results. Our experiments were carried out with very well behaved pulses. Given our ability to eliminate all phase distortions from our pulses, we know they are free from a pedestal or wings. For pulses that have a pedestal, increasing the intensity results in substantially different fields interacting with the molecules and hence to different results. Notice that the results given in Figure 13 were repeated with four different sets of shaped pulses, (a) chirp, (b) binary, (c) the sinusoidal period, and (d) the sinusoidal phase. In all cases, laser pulse intensity had no influence on relative yield. Of course, the signal intensity changed drastically and so did the volume probed in each case; however, the relative yields remained constant for all laser intensities. The overall laser control factors measured were 7.5 for chirp, 11 for binary, 7.5 for the sinusoidal period, and 3 for the sinusoidal phase and were found to be independent of laser intensity. The controllability parameter for chirp modulation here is four times smaller than that found in Figure 11 because for these measurements, the maximum chirp (5000 fs^2) was two times smaller than that in the previous experiment (10 000 fs^2). These results prove that energy density is not responsible for the changes observed in the fragmentation patterns.

5. Dependence of Fragmentation Pattern on the Phase Function Used. As we have seen in Figure 7b and Figure 11a, I−III, neither the sign of the quadratic phase modulation nor the sign of the period of a sinusoidal phase modulation affect the results. However, the modulation parameters do affect the total yield of fragments. It is very interesting that for all types of modulation, we determined the total yield of fragmentation and ratio between heavy and light fragments to be linearly proportional to the measured SHG in the crystal or the total ionization yield, as seen in columns IV and V of Figures 10, 11, and 12.

In order to compare the results among different pulse shaping phase functions, we used the normalized integrated ion signal I_{MS} as an independent parameter, with $I_{MS} = 1$ for TL pulses. The extent of phase modulation causes I_{MS} to decrease. We used

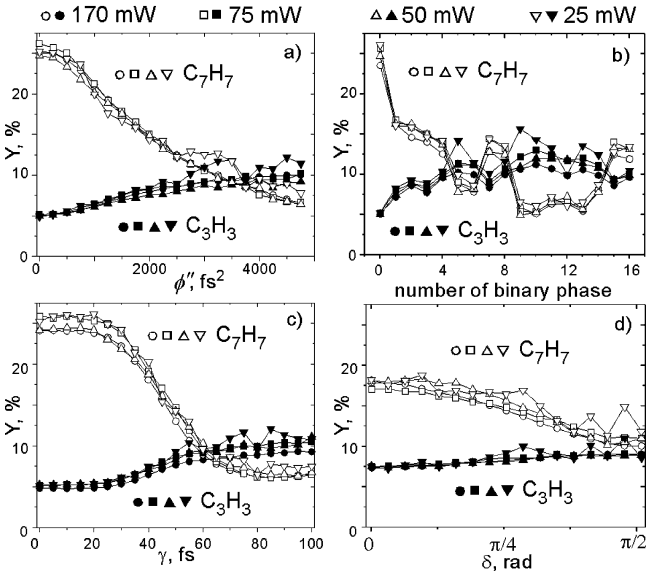

Figure 13. Percentage of total ionization measured at different laser powers (dot, squares, and up and down triangle for 170, 75, 50, and 25 mW, respectively) for two main fragments of the dissociation of *p*-NT, C_7H_7 (open symbols) and C_3H_3 (filled symbols). Experiments were carried out using different types of phase modulation including a) quadratic phase modulation $0.5\phi''(\omega - \omega_0)^2$, b) 8-bit binary phase modulation, c) sinusoidal phase modulation with different period π sin-[$\gamma(\omega - \omega_0)$], and d) periodical phase modulation with scanning phase π sin[35 fs $(\omega - \omega_0) + \delta$]. The difference of the signal for different powers is no more than the standard deviation of the measurements.

different methods of phase modulation, including (a) quadratic phase modulation, $\phi(\omega) = (1/2)\phi''(\omega - \omega_0)^2$, (b) periodic phase modulation, $\phi(\omega) = \alpha \sin[\gamma(\omega - \omega_0)]$, and (c) binary phase modulation, in which the phase number is defined as $\Sigma_i 2^i \phi_i/\pi$. We compare the relative yield of six different $C_nH_n^+$ ions normalized to their yield when using TL excitation and plot them against I_{MS}. In the first column of Figure 14, we present the change in yield for each of these fragment ions for each method of phase modulation. Notice the clear evidence for the elimination of C_2H_2 units is reflected in the alternating intensities of the different fragment ions ($C_7H_7^+$, $C_5H_5^+$, $C_3H_3^+$). In Figure 14, essentially identical trends are observed for every single fragment, despite the use of three very different forms of phase modulation. The similarity in the yields as a function of I_{MS} between the very different pulse shaping experiments is unexpected. We note that the laser control factor is about 5 in the four cases. However, it appears from the second column of Figure 14 that the extent of fragmentation depends on I_{MS} but does not depend on the function used to shape the pulses. As we can see from Figure 4, different types of modulation produce very different fields, but the relative yields of fragments depend only on the overall efficiency of the field to produce ions and not on the detailed temporal or spectral behavior of the field. As observed earlier, this efficiency (I_{MS}) is also proportional to the integrated yield of SHG (I_{SHG}). From Figure 14, we confirm that, in general, as the pulse is shaped, the relative yield of smaller ions increases while that of heavy ions decreases.

6. Statistics of Total Ion Yield and the Ratio between Ion Yields. Our findings so far seem to support the hypothesis that regardless of the pulse shaping phase function, a single laser characterization parameter, such as the resulting I_{MS} or I_{SHG}, can be used to determine the fragmentation pattern and hence the laser control factor for a given ratio between two fragment ions. We devised an experiment that would stringently test this hypothesis. This experiment is unusual because it is designed

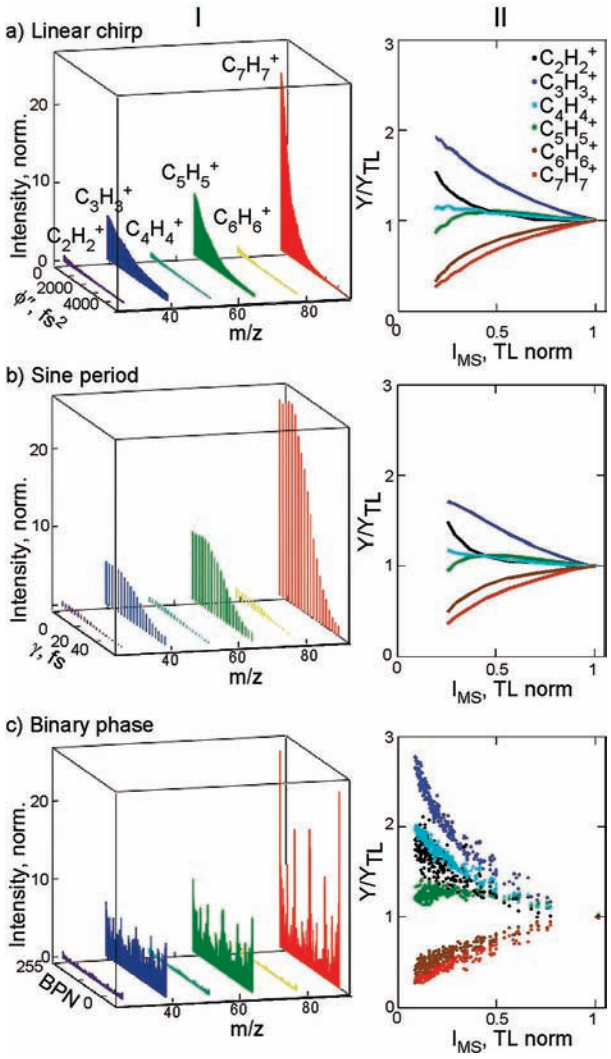

Figure 14. Comparison of effects of different types of phase modulation on fragmentation of *p*-NT. Experiments were done using a) quadratic phase modulation $0.5\phi''(\omega - \omega_0)^2$, b) sinusoidal phase modulation with different periods is $\pi \sin[\gamma(\omega - \omega_0)]$, and c) 8-bit binary phase modulation. In column I, mass spectra of selected ions (C_nH_n) are presented as functions of the scanning parameters of phase modulation. In column II, the intensity of selected lines is presented as a function of the total fragmentation yield, with the data on both axes normalized to the value under TL excitation. The difference between normalized functions is no more than the precision of the measurements.

to find any pulse that violates the hypothesis. This requires us to evaluate an entire set of pulses that have a particular I_{MS} and I_{SHG} and determine if any show a different fragmentation pattern, as would be evidenced by a product ratio that differs from others by more than the experimental noise.

For this experiment, we used shaped pulses with precalculated (10-bit) phase functions that generate only 10−20% of the SHG corresponding to TL pulses. In these experiments, we used a limited range of the available spectrum. The wings of the spectrum were suppressed to produce a shape that more closely resembles a flat spectrum. For our simulations, we used Galois fields, where the spectral component of the electric field can only be positive or negative at the flat spectrum.[74] Statistical analysis of 537 different phases is presented in the Figure 15. For all of the hundreds of measurements, a linear dependence of I_{MS} versus I_{SHG} is observed; see Figure 15a. The statistical signature for linear dependence is the Pearson correlation coefficient (r), which is very close to unity for this experiment.

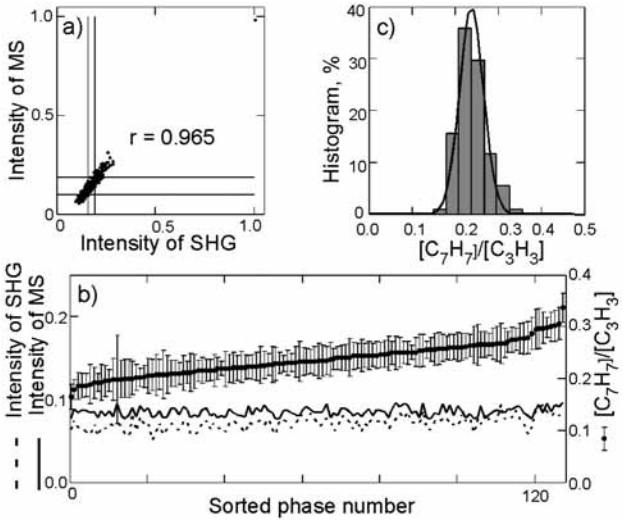

Figure 15. Statistical analysis of the total yields of fragments and the ratio between selected fragments for 537 different types of binary phase functions. a) Total yield of all ions as a function of the corresponding SHG intensity. The lines delineate the region for which 128 different shaped pulses are within the standard deviation of our measurements and were chosen for further analysis. b) Ratio between the yields of masses 91 and 39 (points with error bars) together with the total intensity of the mass spectrum (solid line) and SHG (dotted line) sorted in ascending order of ratio. c) Histogram of the ratios in panel b. Notice that all measurements fall within the Gaussian noise spectrum that is consistent with the standard deviation of our measurements.

In Figure 15b, we show results for all experiments that fell inside of the window for I_{MS} and I_{SHG} defined by the standard deviation of experimentally measured I_{MS} and I_{SHG}. We sorted these measurements according to ascending ratio. All of the phase functions produced MS spectra with a ratio of $[C_7H_7]/[C_3H_3]$ described by a normal Gaussian distribution shown in Figure 15c. This agreement between the measurements and the predicted value implies that statistically there is no difference in the selectivity of the fragmentation outcome as a result of phase modulation, regardless of the binary phase function used.

7. Dependence of the Mass Spectrum on Different Shaped Pulses. For these experiments, we compared the MS spectra for a number of very different phase-modulated pulses, all producing the same I_{SHG} and I_{MS}. These measurements were designed to test if I_{SHG} was reliable for predicting the fragmentation and ionization of *p*-NT. In Figure 16, we show the raw MS spectrum for each of the laser pulses. Different types of modulations were used, including binary phase modulation ($\pi\pi\pi00\pi\pi\pi$), positive and negative linear chirp (± 2650 fs^2), and periodical phase modulation of different sign ($\pm\pi \sin[35$ fs $\times (\omega - \omega_0)]$. The calculated time−frequency behavior of the pulses, the Wigner function, is shown in Figure 17. The time profiles for these pulses are very different, but all of them generate one-fourth the SHG of TL pulses. As was shown above, the total ion yield is directly proportional to the total SHG, and in these experiments, the total yield of all ions is (1/4) of the yield generated by TL pulses. As we can see from Figure 16, the MS of ions generated by these very different five pulses are indistinguishable (maximum of 20% deviation in the laser control factor for $[C_7H_7]/[C_3H_3]$) despite very different time−frequency behavior of the five different fields. Given that we are able to achieve more than an order of magnitude control in this ratio, we consider this 20% difference insignificant. The maximum deviation observed was between binary and sinusoidal modulation. A reason for the deviations caused by binary phases is discussed below.

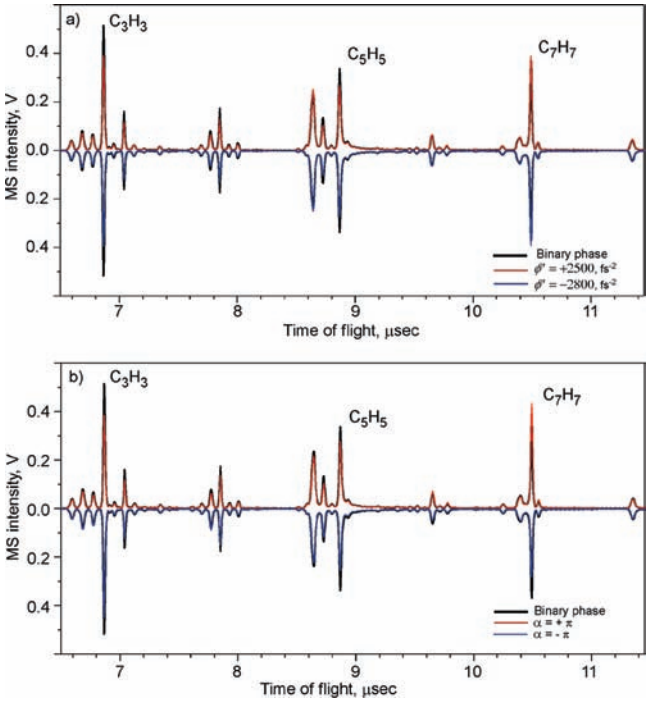

Figure 16. Raw oscilloscope traces measured from our TOF MS showing part of the mass spectrum of *p*-NT obtained for different types of phase modulation that yield one-forth of the ions that are observed for TL excitation. The black line in both panels corresponds to the MS for binary phase modulation, when the phase is evenly modulated in the frequency domain with the binary string $\pi\pi\pi00\pi\pi\pi$. a) Red and blue lines are for positive and negative chirped pulses $\phi = \pm(1/2)\phi''(\omega - \omega_0)^2$. b) Red and blue lines are for the positive and negative sinusoidal phase function $\phi = \pm\alpha \sin[35 \text{ fs } (\omega - \omega_0)]$. All phase modulations are found to result in a fragmentation pattern that depends only on the total yield of all fragments relative to TL excitation.

8. Predictability of Mass Spectra for *p*-NT. On the basis of our observations above, we propose that each molecule undergoes a characteristic photofragmentation sequence that is activated by the laser pulse and varies monotonically with a laser parameter, which, in this case, we quantify by I_{SHG} or I_{MS}. This implies that the extent of pulse shaping, measured as the normalized I_{MS} or I_{SHG}, will allow one to predict the resulting mass spectrum regardless of the phase function used to modulate the pulse (chirp, sinusoidal, etc.).

We tested this predictability hypothesis on *p*-NT by subjecting it to a number of intense pulses shaped with different phase functions. For all cases, the results obtained as a function of linear chirp (see Figure 18) are plotted as a line. Results from (a) different periodicity of the sinusoidal modulation, (b) the location of the phase mask δ, (c) split pulses in the time domain, (d) binary phase modulation, (e) hundreds of pulses with different arbitrary phase modulation, and (f) hundreds of different phases resulting from a Taylor expansion series are plotted as a function of I_{MS}. We find that the fragmentation in all cases is very similar to that found for linear chirp (lines). The visible systematic deviations (20−30%) for the different phase modulation observed (for case (c), values obtained for $I_{MS} < 0.4$) and for the discontinuous phases are caused by slight amplitude changes that occur when discontinuous phase functions are implemented on the SLM. The effects of amplitude and phase−amplitude modulation are discussed in the next subsection. The data in Figure 18 reveals that for any phase-shaped pulse, if we know the normalized I_{SHG} or I_{MS}, we can predict the resulting mass spectrum within a few percent. Similarly, we expect that each molecule will have a monotonic

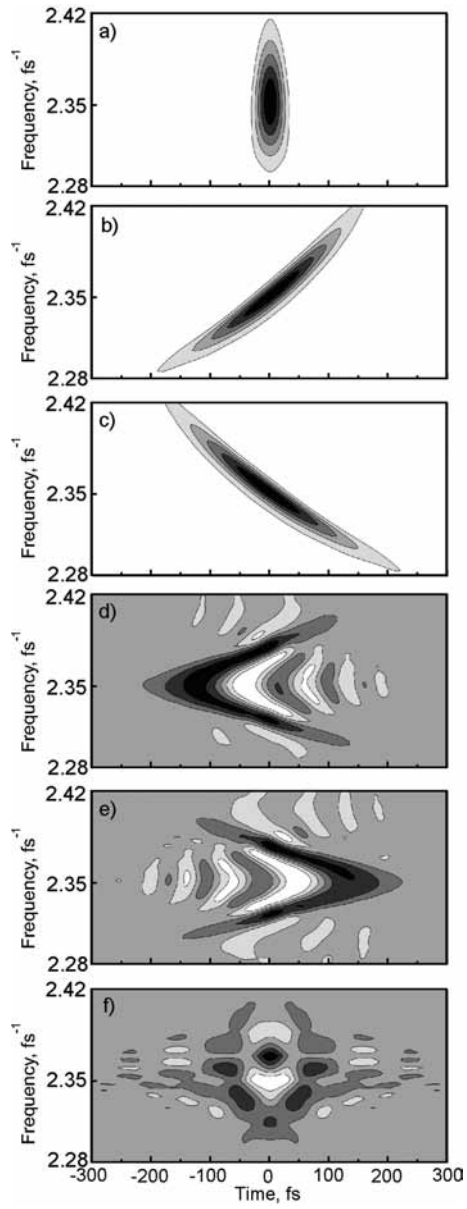

Figure 17. Calculated Wigner functions of the phase-modulated femtosecond laser pulses, used for Figure 16, in the time and frequency domains. a) Phase-compensated TL pulse. b) and c) Positively and negatively chirped pulses with phase function $\phi = \pm(1/2)2500\text{fs}^2(\omega - \omega_0)^2$. d) and e) Laser pulse with sinusoidal phase function $\phi = \pm\pi \sin[35 \text{ fs } (\omega - \omega_0)]$. f) Binary phase modulation when the phase is evenly modulated in the frequency domain with binary string $\pi\pi\pi00\pi\pi\pi$.

fragmentation pattern, which once determined by a linear chirp dependence, for example, will allow one to predict the resulting mass spectrum for any phase-shaped pulse.

In order to have a more complete evaluation, we designed a set of orthogonal polynomial functions inspired by the first five states of a harmonic oscillator. Evaluation of that entire search space with thousands of combinations yielded results that are consistent with those found for the other phase functions shown in Figure 18, therefore they are not shown.

9. Effects arising from Spectral Amplitude Shaping. In all of the measurements presented (Figures 10−12), I_{MS} was found to be proportional to I_{SHG}. Here, we explore if this direct proportionality applies to amplitude shaping. The measurements obtained for 256 8-bit binary amplitude-shaped pulses, for which the amplitude of different pixels was set to 0 or 1, are presented in Figure 19. We plot the dependence of I_{MS} and I_{SHG} versus

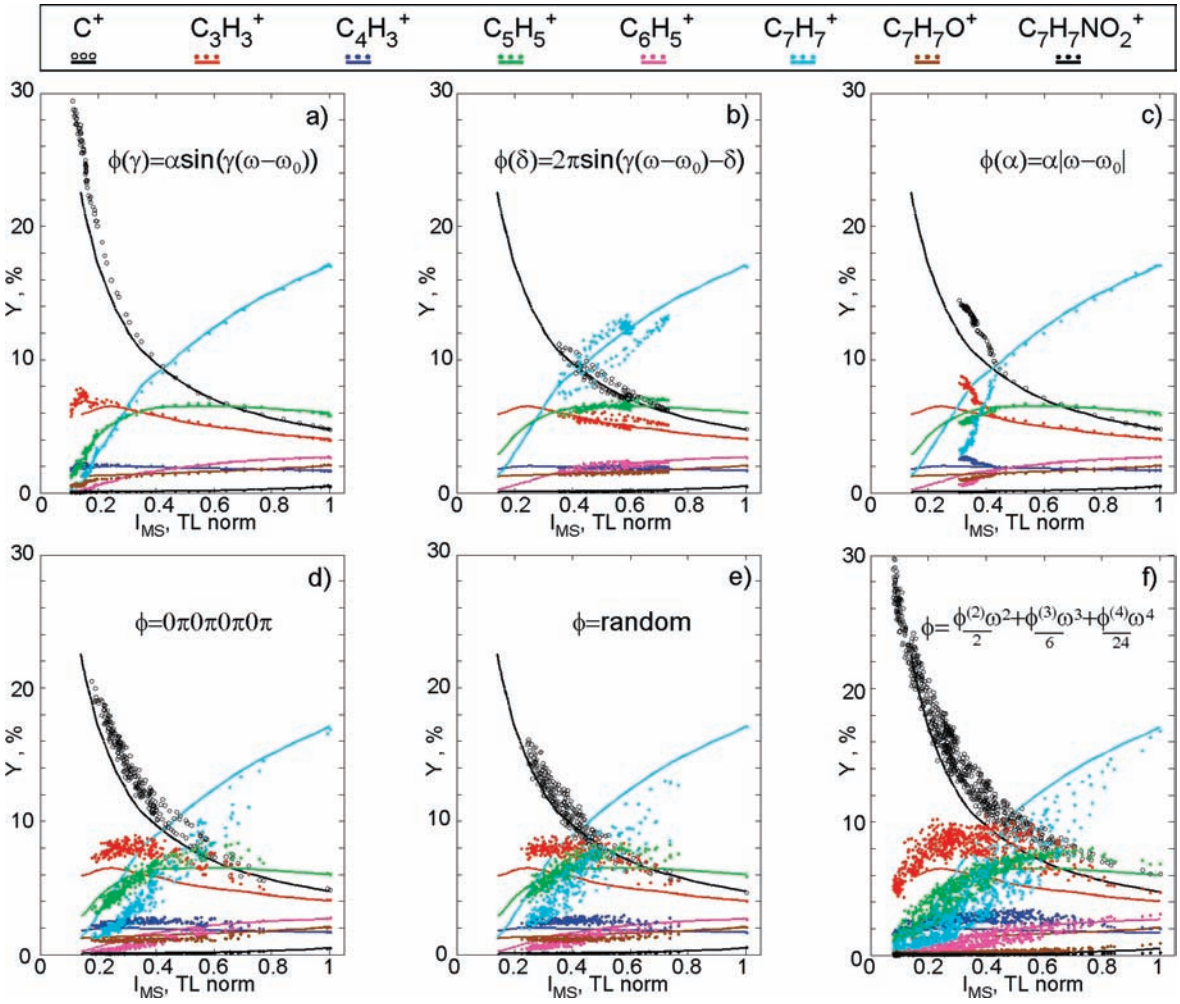

Figure 18. Relative intensities of some MS lines (Y) of *para*-nitrotoluene plotted as functions of the relative total intensity, I_{MS}. The graphs show the comparison of different types of phase modulation (points) with quadratic phase modulation of different positive chirp values from 0 to 10 000 fs^2 (lines). a) Sinusoidal phase modulation $2\pi \sin[\gamma(\omega - \omega_0)]$ with different positive periods γ from 0 to 200 fs. b) Sinusoidal phase modulation $2\pi \sin[35 \text{ fs } (\omega - \omega_0) - \delta]$ with different phase delays δ from 0 to 4π. c) Phase modulation with function $\alpha|\omega - \omega_0|$, which provides splitting of the pulse to the two parts with delay time (2α) from -800 to 800 fs. d) Full set of 256 phases of binary ($0,\pi$) phase modulation by binning 8 pixels per bit in the central part of the spectrum. e) 256 random phases from 0 to 2π by binning 8 pixels over the whole spectrum. f) All possible combinations of three terms of the Taylor expansion, where the nonlinear terms of the expansion are in the range of $\pm 1.6 \times 10^4$ fs^2, $\pm 8 \times 10^5$ fs^3, $\pm 4 \times 10^7$ fs^4 for the second, third, and fourth orders of phase modulation, respectively. There is a minor quantitative difference found for discontinuous phase functions, but the fragmentation pathways always vary monotonically as a function of I_{MS}.

the intensity of the fundamental pulse in Figure 19a. From the log−log plot, we find that I_{MS} has close to fourth-order dependence on the intensity of the fundamental pulse. This observation is unexpected given the well-known square dependence of I_{SHG} on $I_{Fundamental}$. The difference in this experiment is that the binary amplitude modulation causes both a loss in intensity of the fundamental and a lengthening of the pulse. The twofold effect causes a nonlinear dependence with $n > 2$. We confirmed by numerical simulation that the intensity of SHG generated by binary amplitude-modulated pulses is proportional to the intensity of the fundamental pulse in the order of $n = 3$ to 4, where the smaller number corresponds to a single block of bits set to 0 and the larger number is found for amplitude functions with alternating on−off bits. These values are in agreement with the data measured. Our amplitude modulation measurements are very different than pulse attenuation, where all frequencies are attenuated by a certain amount. In that case, the familiar $n = 2$ dependence is observed. We note in Figure 19a that I_{SHG} (red dots) and I_{MS} (blue dots) have exactly the same dependence on $I_{Fundamental}$, as observed earlier for phase modulation. In Figure 19b, we plot the intensity of two individual fragment ion peaks with m/z of 91 and 39 as a function of I_{SHG}. In the log−log plot, we see that the dependence is to the fourth power at the lowest intensities, but it quickly saturates and reaches linear dependence. The change may be a signature of different mechanisms of ionization/fragmentation for low and high intensities.

Experiments on laser control have usually combined phase and amplitude modulation, with the hope that this more general combination will optimize a desired quantum mechanical pathway. When the system being controlled can be excited linearly by the laser (resonant excitation), amplitude modulation controls the population transfer to every excited state within the laser bandwidth. When the excitation is through a nonlinear interaction, for example, multiphoton excitation, phase can be used to control the amplitude at specific frequencies very efficiently without amplitude modulation (loss of photons).[60,61] Here, we explore the combination of phase and amplitude modulation systematically for *p*-NT (a molecule without excited states within one-photon excitation by the laser) to find if there is a departure from pure phase modulation. For these experiments, we tested 32 different 5-bit amplitude-modulated pulses (using pulse shaper II), and for each, we measured mass spectra

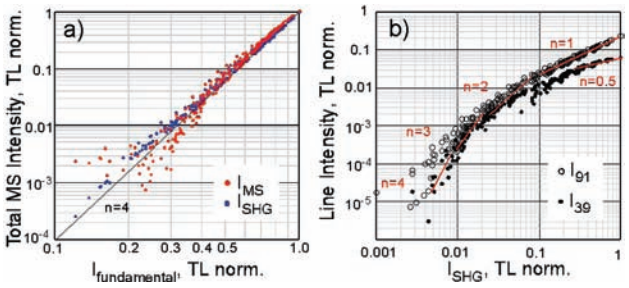

Figure 19. a) Dependence of the total yield of fragments (red) and SHG from a crystal (blue) as a function of pure binary amplitude modulation, plotted as a function of laser intensity. b) Intensity of the fragments ions with *m*/*z* 91 and 39 of *p*-NT as a function of the SHG intensity obtained for the amplitude modulation experiments.

for 50 different phase functions (introduced by pulse shaper I) using quadratic phase modulation from 0 to 10,000 fs^2. The results from these measurements are plotted in Figure 20. First, we find in Figure 20a that the total ion yield, I_{MS}, is essentially linear with the integrated SHG intensity, similar to the results shown earlier for all phase modulation experiments.

In Figure 20b, we plot the percentage of total ionization measured for *m*/*z* 91 and 39. The lines correspond to a laser without amplitude modulation. The first observation is that amplitude modulation causes an overall shift in the relative ion yield curves, but the changes in relative yield are systematic and follow the same monotonic trend as that found for all of the previous experiments above. This suggests to us that there is no quantum mechanical pathway that has been blocked by the amplitude modulation. In a sense, the amplitude modulation is working as an additional pulse-lengthening effect that shifts the dependence on I_{MS} but does not affect the fundamental fragmentation pathways. The second observation is that the changes in the trends, lower values for *m*/*z* 91 and higher values for *m*/*z* 39, are consistent with the observation in subsection 8, where heavily modulated pulses and discontinuous phase functions were found to deviate from the trends observed for chirped pulses. The experimental data in Figure 20b, therefore, give us the confidence to claim that there was nothing special in the experimental points that deviated from the trend when discontinuous phase modulation functions were used (see Figure 18). The deviations were caused by inadvertently introduced amplitude modulation.

10. Generalization of Our Findings to Other Molecules. To further test our hypothesis that the laser-induced fragmentation and ionization pattern can be predicted once we learn how it depends on I_{MS}, we explored the behavior of 16 different molecules upon pulse shaping with two very different phase functions. In Figure 21, we compare the total ion yield I_{MS} for quadratic phase modulation (continuous line, where ϕ'' was up to 10 000 fs^2) and for sinusoidal phase modulation (dots) given by $2\pi \sin[\gamma(\omega - \omega_0)]$, where γ is scanned from 0 to 100 fs. First, we observe that I_{MS} is directly proportional to I_{SHG} for all molecules and is practically independent of the phase function used.

Next, we explore the fragmentation patterns for the 16 different molecules and test the observations, made for *p*-NT, that it changes monotonically and predictably as a function of I_{MS} despite the phase function used to shape the pulses. The data is shown in Figure 22, where the relative product ion yields measured for the linear chirp (lines) and the period of a sinusoidal function (dots) are found to be practically identical when plotted against I_{MS}. Some slight deviations are observed when pulse shaping is such that less than 0.3 of I_{MS} is detected; this is caused

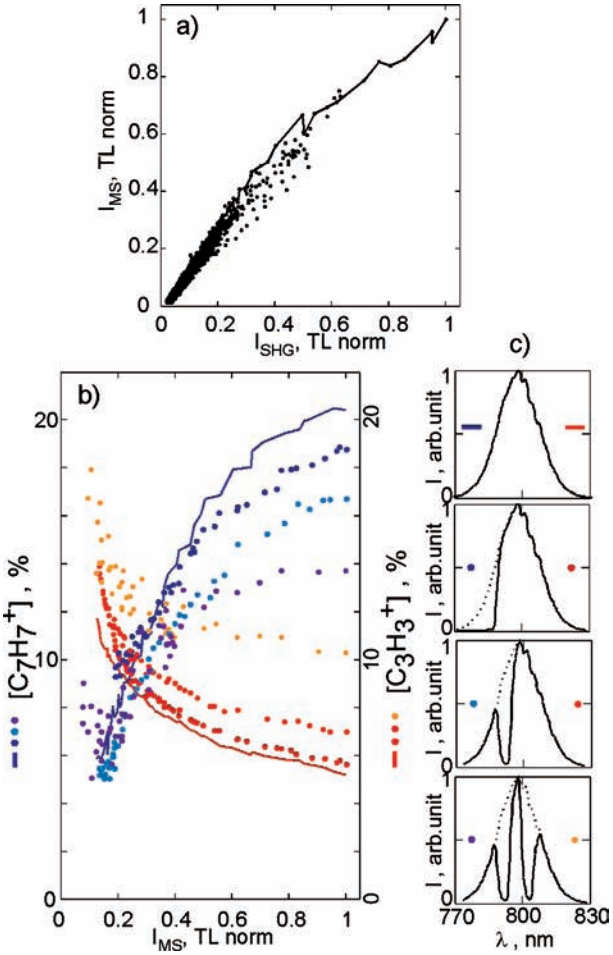

Figure 20. a) Total fragment ion yield as a function of the total SHG intensity for amplitude- and phase-modulated pulses. b) Percentage of the total ionization of fragments with *m*/*z* 91 (blue colors) and 39 (red colors) for *p*-NT as a function of the total ion yield normalized for TL excitation. c) Spectra of the amplitude-modulated pulses corresponding to each case. The solid line corresponds to results obtained without amplitude modulation, as shown in the top spectrum in (c).

by unwanted amplitude modulation, as discussed above. We carried out experiments with other phase functions such as binary Taylor expansion, and for all of the molecules, the results were essentially the same as those presented in Figure 22. The results of these experiments strongly support our conclusion that the fragmentation pattern varies monotonically and predictably with I_{MS}. Once the fragmentation pattern as a function of I_{MS} has been determined, as shown here by scanning linear chirp, then this function can be used to predict the fragmentation pattern for any other shaped pulse based on its I_{MS} value.

The data in the first three panels of Figure 22 illustrate how the yield of particular fragment ions changes for molecular isomers. For example, the molecular ion of *m*-NT is much more sensitive to pulse duration than that from *p*-NT (Figures 22.1 and 22.2). The intramolecular proton transfer reaction that leads to *m*/*z* 120 changes by two orders of magnitude for *o*-NT. More examples of isomer identification have been discussed elsewhere.[32,40,75] Differences in the femtosecond laser mass spectra of isomers are not new (see, for example, refs 42, 44, and 76−78). What is new is that by shaping the pulse, we can distinguish one molecule from another by the changes in the yield of a single fragment ion. Here, we see that the relative yield of a fragment with *m*/*z* 39 responds differently to pulse shaping. For the nitrotoluenes (Figure 21.1−3), it decreases with increasing I_{MS}; for chlorobenzonitrile, it is insensitive to pulse shaping

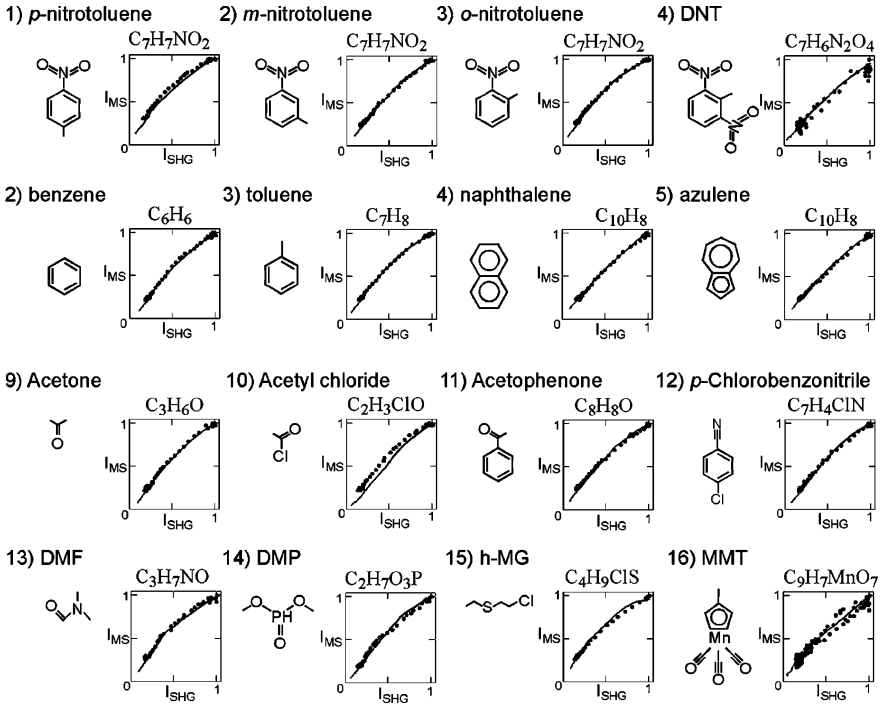

Figure 21. 1)−16) Total yield, I_{MS}, as a function of SHG intensity, I_{SHG}, measured for 16 different molecules. Comparison of the linear chirp when ϕ'' is scanned from 0 to 10 000 fs^2 (lines) with periodical phase modulation $2\pi \sin[\gamma(\omega - \omega_0)]$ for γ scanned from 0 to 100 fs (points).

(Figure 21.12), and it increases for benzene (Figure 21.5). These differences can be used for molecular identification purposes.[32−36,40,75] A parameter that integrates the changes in the molecular response upon pulse shaping, for example, measuring variance, allows us to add an extra dimension to mass spectrometry that can be used to improve molecular identification.[41]

One of the molecules tested was acetophenone (shown in Figure 21.11), a molecule that had been studied with shaped laser pulses.[19−21] Notice that no toluene (*m*/*z* 92) was observed for any of the different pulses, in contradiction to the experiments reported by Levis et al.[19,20] The appearance of *m*/*z* 92 as well as other unexpected lines is explained elsewhere.[79]

11. Intensity and Volume Effects. When our experimental findings for *p*-NT were presented at a laser control conference, they generated concern among some colleagues that our observations were merely a volume effect. Experiments in strong fields, especially when the laser intensity exceeds I_{sat}, are performed with lasers having a Gaussian intensity profile; therefore, the signal obtained contains a range of intensities. Higher intensities are reached only in the center of the beam and produce a minor contribution, while the greater volume outside of the focus produces a major contribution. Taking into consideration that changing the laser Rayleigh parameter as shown in Figure 9, changing the laser intensity as shown in Figure 10 (top row), and changing the laser intensity as shown in Figure 13 caused no difference in the observed laser control as a function of pulse shaping gives us confidence that volume effects are not responsible for the observed changes in fragmentation patterns. However, in light of the concern, we carried out additional experiments to evaluate to what extent our findings could be influenced by volume effects. The method we used is based on the observation by Ben-Itzhak that for Gaussian beam profiles, when collecting data through a slit perpendicular to the laser excitation, subtraction of lower intensity data can be used to isolate effects caused by the higher excitation.[73] This method has been tested and is rigorous for two-dimensional slices when using Gaussian pulses.

Two-dimensional volume effects were explored using the long focal length setup with a 0.9 mm slit perpendicular to the beam propagation. These parameters are well in the range required for eliminating volume effects by subtraction.[73] First, we measured the yield of three different fragment ions as a function of power density (data shown in Figure 23). We confirmed that I_{sat} for *p*-NT is about 10^{14} W/cm^2. Having the power dependence, we were then in a position to evaluate the differential changes in ion yield for the different fragment ions. These findings, shown in the top row in Figure 23, show two regimes. Below I_{sat}, there is a systematic rise in the appearance of the ions. Above I_{sat}, there appears to be no significant change outside of the noise in the yield of these fragments. Note that with this being a differential measurement, it is very sensitive to noise.

We also explored volume effects that may have played a role for the short focusing geometry. In this case, given the very short Rayleigh length, we did not use a slit. Although this case is outside of the two-dimensional geometry, it still allows us to explore possible volume effects. Once again, we find in these data, shown in the bottom row of Figure 23, that beyond I_{sat}, differential increases in energy cause essentially no change in the yield of the different fragment ions. Given the order of magnitude changes in the relative fragment ion yields reported in our study as a function of pulse shaping, the minimal change in the differential yield gives us some confidence that the observed effects on pulse shaping are not caused by volume effects, in either of the focusing configurations explored in this work.

Having determined that volume effects have little or no effect on controlling fragmentation selectivity in our experiment above I_{sat}, we measured the effect of pulse shaping (sine function open circles and chirp filled circles) at different laser intensities (data shown in Figure 24). These data were obtained using the longer focal length geometry. At the higher intensities, our data reproduce the results found earlier, namely, extensive changes in the yield of $C_nH_n^+$ fragment ions upon pulse shaping. At I_{sat}, we find that the effect of pulse shaping is essentially lost.

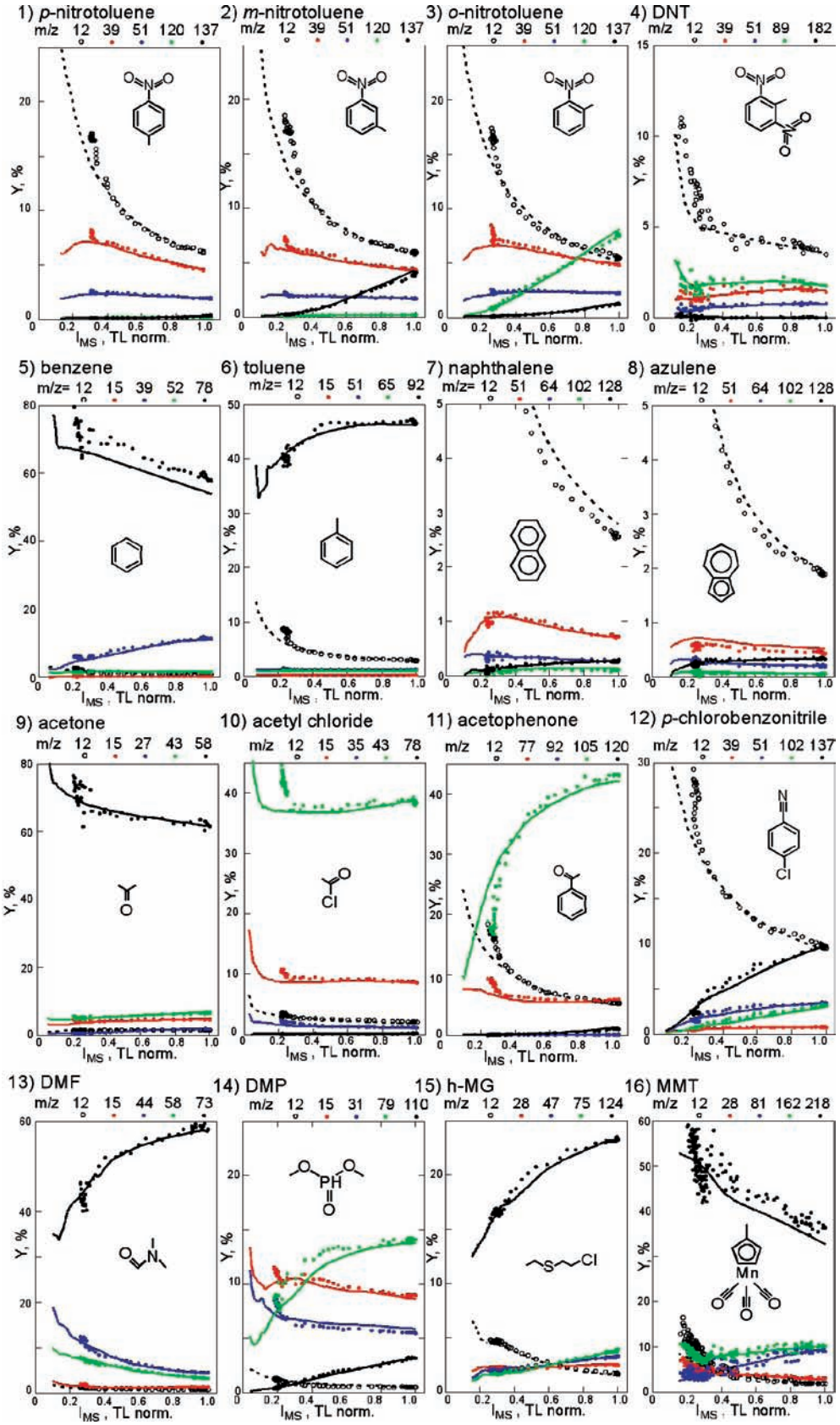

Figure 22. (1−16) Relative intensity of the most prominent MS lines (Y), including C^+ (open black) and the molecular ion (black dot) as a function of the total yield of all ions (I_{MS}) for 16 different molecules as a function of linear chirp when ϕ'' is scanned from 0 to 10 000 fs^2 (lines) and as a function of periodic phase modulation $2\pi \sin[\gamma(\omega - \omega_0)]$ for γ is scanned from 0 to 100 fs (points).

Finally, at very low intensities, we find that noise overwhelms the possible changes as a function of pulse shaping. More importantly, for all three laser intensities we find no difference arising from the use of two different phase shaping functions.

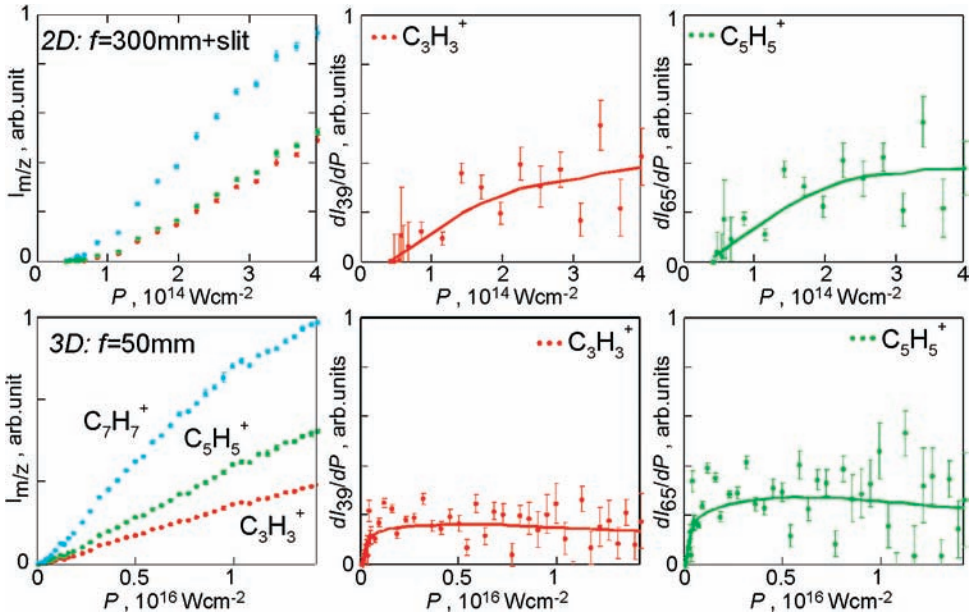

Figure 23. Volume effect. The dependence of the relative yield of three fragments *m*/*z* 39, 65, and 91 from *p*-NT as a function of power density. Upper row: The experiment was carried out using a 300 mm focal length lens and a 0.9 mm slit in the extraction plate. Lower row: The experiment was carried out using a 50 mm focal length lens and mesh in the extraction plate. The lines are smooth functions obtained from the experimental points.

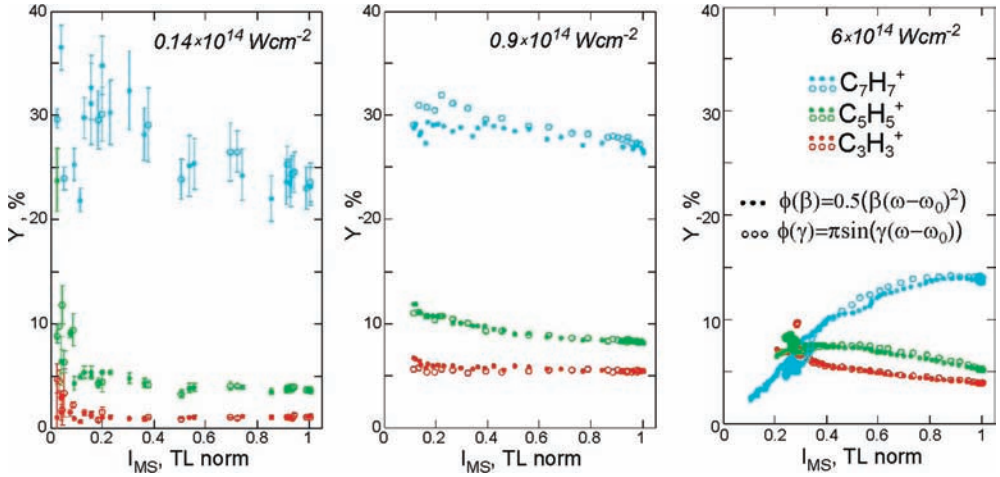

Figure 24. Controllability of fragmentation at different power densities. The dependence of the relative yield of three fragments *m*/*z* 39, 65, and 91 from *p*-NT were measured as function of the integrated yield of all ions, I_{MS}, for different power densities using chirped pulses (filled dots) and sinusoidal phase modulation with a different period (open cycles). Note that at the three different power densities, the fragment ion yield is independent of the type of phase modulation used.

Discussion

1. Femtosecond Laser-Induced Photochemistry of *p*-NT. The photochemistry of *p*-NT[80−87] and its analogue nitrobenzene[88−98] have been the subject of intensive research, with some results that have been considered controversial, but the major transformations are well established. We present our findings in light of the more widely accepted model for the fragmentation of *p*-NT and the ladder switching mechanism shown in Figure 25. This model can be rationalized using one or more models of photoionization and photodissociation collected in Table 1. The first step occurs in the rising edge of the pulse and involves field ionization. We have measured the threshold for field ionization at 800 nm for *p*-NT to be 1.7×10^{14} W/cm^2, a number that is reasonable given the literature,[66,67] where a large number of experimental and theoretical values for field ionization thresholds are collected. Only for pulses with heavy amplitude modulation, where we simultaneously reduced the fundamental amplitude by 5 times and increased the pulse duration by 10 times, does the intensity become lower, and a deviation from the typical fragmentation pattern becomes apparent (see Figure 18a). For the shortest and most intense pulses, we observed the signature of double ionization and Coulomb explosion (see Table 1), and this data, representing <5% of the total ion yield for the highest intensity experiments, is discussed later.

The observed low relative yield for the molecular ion seems to indicate that the parent ion is unstable. However, we know from electron impact MS (see Figure 2a) that the parent ion is stable. Therefore, differences between electron impact and femtosecond ionization indicate that the molecular ion is not stable in the presence of the laser field. We confirmed this observation by comparing the mass spectrum of *p*-NT obtained with 35 fs TL pulses at peak intensities of 10^{13} and 10^{14} W/cm^2 (see Figures 6b and c). At the lower intensity, the parent ion reaches as much as 30% relative yield; this value decreases with laser intensity.

After *p*-NT is field ionized, we observe that I_{MS} is linearly proportional to the SHG intensity, I_{SHG}, suggesting that a two-photon bottleneck exists, and it is plausible that it is related to the loss of the molecular ion. For *p*-NT, the isomerization in which CH_3-ϕ-NO_2 transforms to CH_3-ϕ-O−NO has been found to have an energy barrier and does not take place in solution. This energy is supplied by the strong laser field. Experimental data and calculations reveal that one 800 nm photon is not enough to form the isomer, but two photons are sufficient for isomerization. As a result, the *p*-NT ions undergo isomerization, which promptly results in the elimination of NO or NO_2. Under thermal equilibrium, the main channel is NO elimination, followed by sequential CO elimination. In the presence of a strong field, the preferred decay channel is NO_2 elimination, while under electron impact, the molecular ion is stable. After NO_2 elimination, the $C_7H_7^+$ ion, initially in the benzyl form, appears and transforms into the more stable seven-member ring, the tolyl ion, which is most likely the form that is detected. In the presence of the strong electromagnetic field, sequential absorption of photons releases C_2H_2 fragments, thereby forming the $C_5H_5^+$, $C_3H_3^+$, and finally C^+ ions. The observation that longer pulses (with a lower I_{SHG} and/or I_{MS}) produce more fragmentation can be understood dynamically. The longer the pulse, the more time the atoms have to change their configuration. When plotted against chirp, as in Figure 14a, the relative intensity of smaller fragments increases with chirp, the larger fragments decreases with chirp, and intermediate fragments, like $C_5H_5^+$, first increases and then decreases. The observed fragmentation mechanism is consistent with ladder climbing followed by ladder switching. For the longer pulses, the field remains sufficiently strong to cause the formation of fragment ions by ladder switching processes.

For *p*-NT, the fragmentation pattern from electron impact mass spectrometry is very similar to the fragmentation pattern observed for femtosecond pulse excitation below I_{sat}. This similarity makes us consider the electron recollision (ERC) model in Table 1, might play an important role in the laser-induced fragmentation and ionization process. We would expect ERC to play a greater role for TL pulses for which post-ionization excitation is expected to be minimal. We examined the fragmentation pattern as a function of polarization for TL pulses. By changing the polarization from linear to circular, we would expect to modulate the probability of electron−nuclei collisions in analogy to the high-harmonic generation process.[116] We found that these change in polarization did not affect the fragment ion pattern. This suggests that ERC does not play a major role in determining the fragmentation pattern in our experiments or that electron−nuclei collisions are not needed for the electron to transfer energy to the molecule.

A number of models have been proposed that consider multielectron excitation (IED, MDI, and NME in Table 1). It is possible that multielectron excitation is favored by shaped pulses, which are longer and therefore lead to further fragmentation. We had expected that certain shaped pulses would enhance specific pathways when specific electronic excitation pathways are accessed. However, we have found no evidence that such selective excitation takes place for any of the different shaped pulses used. We have sufficient evidence to suggest that sinusoidal δ scanning and binary phases would result in excitation of multiphoton processes at different wavelengths. However, no evidence for having accessed different electronic states is present in the fragmentation patterns observed. Similarly, we tested several pulse shapes, such as sinusoidal functions

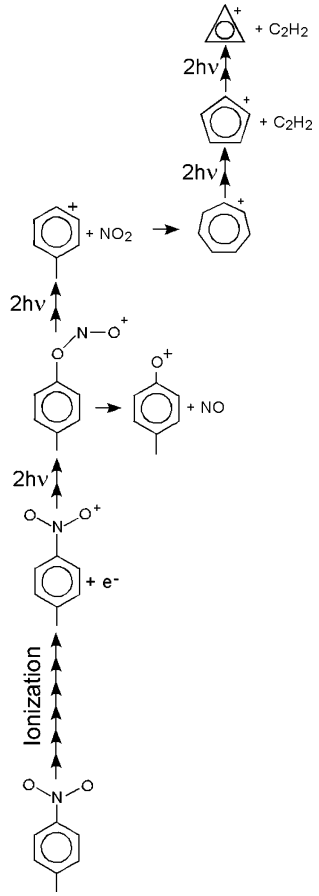

Figure 25. Ladder switching mechanism of the photodissociation of *p*-NT upon femtosecond IR excitation. The first step is fast field ionization. The second step is photoisomerization, from which NO or NO_2 elimination takes place, followed by further steps involving C_2H_2 loss. Pulse shaping enhances ladder switching processes, while TL pulses enhance ladder climbing.

TABLE 1: Models of Ionization and Dissociation in Femtosecond Fields

#		models of dissociation	molecules and references
1	ADI	dissociation followed by ionization	C_3H_6O[105] NO_2[106]
2	AID	ionization followed by dissociation	C_6H_6[107] C_nH_m[108] $C_nH_mCl_kF_l$[109] $M(CO)_n$[110] C_3H_6O [105] $C_3H_3OF_3$[105] C_8H_8O[105]
3	CE	coulomb explosion	C_2H_4[111,112] C_3H_6[111,112] C_2H_6O[113] CH_4O[114]
4	ERC	electron recollision	H_2[115] CH_4[39] C_6H_6[116,117] C_7H_8[63] H_2O[117] CH_4O[118] C_2H_4O[118] $C_6H_{14}O$[118]
5	FAD	field-assisted dissociation	CH_4[119] C_2H_4O[120] CH_2I_2[121] $C_2H_6O_3$[122]
6	FID	field-induced dissociation	C_6H_6[123,124] C_6H_5X[123] $C_{10}H_8$[123] $C_{14}H_{10}$[123]
7	IED	inner valence electron excitation	CH_4[125] C_6H_6[126]
8	MDI	multielectron dissociative ionization	H_2[127] N_2[127] O_2[127] Cl_2[127] I_2[127] CH_3I[128] C_3H_7I[128] C_4H_9I[128] C_6H_8[76,129]
9	NCL	nonadiabatic charge localization	$C_{14}H_{10}$[130]
10	NED	nonadiabatic excitation−dissociation	C_6H_6[131,132] $C_{10}H_8$[131,132] $C_{14}H_{10}$[131,132] $C_{18}H_{22}$[131,132] $C_{14}H_{12}$[131,132] $C_{14}H_{18}$[131,132]
11	NME	nonadiabatic multielectron excitation	C_6H_8[133,134] $C_{10}H_{12}$[133,134] $C_{40}H_{56}$[133,134] C_8H_8[133,134]

that create trains of pulses, with the idea of driving a vibrational coherence. No evidence of coherent vibrational motion was found.

Developing a precise model of ionization and fragmentation for *p*-NT is beyond the scope of this article. We hope that our complete data will encourage scientists to provide a model that will explain the entire mechanism for photoionization and fragmentation. Here, we focus on the main observation of our study. The detailed time−frequency dependence of the shaped laser pulses plays a minor role (if any) in influencing the fragmentation pattern. We have carried out thousands of experiments, trying to find evidence of one or more specially shaped pulses that are capable of causing bond-selective fragmentation of *p*-NT to yield one or two product ions in a pattern that deviates from that which is observed as a function of chirp. We saw no evidence for such a pulse in any of our experiments. This prompts us to propose a model for fragmentation−ionization by intense and shaped near-IR pulses. In this model, the molecular fragmentation pattern, or fragmentation sequence, that depends on their atomic and electronic structure. In this proposed model, the yield of all fragments is interrelated. TL pulses will maximize the observation of the heavier fragments, including the molecular ion if stable under laser irradiation. The longer the shaped pulses, the more extensive the fragmentation sequence will be in producing smaller fragments down to single-atom ions. This can be understood in terms of a ladder switching model. The increased fragmentation observed for shaped pulses can also be interpreted in terms of a dynamic energy flow from the Franck−Condon excited states to hundreds of degrees of freedom, this flow reaching all parts of the molecule when the pulses are lengthened by pulse shaping. In order to predict how far in the fragmentation sequence the molecule will follow, it is sufficient to know I_{MS} or I_{SHG} normalized to TL. All of our measurements with phase-shaped pulses confirm this model. This model envisions the creation of a wave packet encompassing thousands of quantum (rotational, vibrational, electronic, and translational) states, which undergoes ultrafast delocalization. The speed of delocalization reduces and perhaps eliminates the possibility of a time-dependent interplay between the complex laser pulse and the molecular dynamics.

2. General Observation on Pulse Shaping and Fragmentation and Possible Applications. Our results indicate that the photo fragmentation pattern of molecules is determined by their atomic and electronic structure. In Figures 22.1, 22.2 and 22.3, we see that different isomers have very different fragmentation patterns. The fundamental reason for this can be traced back to the restricted energy flow (IVR) which depends on molecular geometry (selection rules).[99] From a practical point of view, this implies that shaped pulses can be used as a tool for analytical chemistry, such as for isomer identification.[75] In order to maximize reproducibility and minimize the number of shaped pulses used, we stress the need for elimination of phase deformations in the laser system to ensure TL pulses at the sample. Measuring the outcome from two shaped pulses allows quantitative identification of mixtures.[75] Phase functions that can be reproduced accurately will give the most reliable and reproducible results.

The spectra shown in Figure 22 contain a wealth of information. We find that for certain molecules, such as acetone, acetyl chloride, benzene, and toluene, the fragmentation pattern is relatively insensitive to pulse shaping when compared to that of the rest of the molecules. We also find that the fragmentation of azulene and naphthalene, molecules with very different spectroscopy and ionization potentials, is quite similar. We note that for acetone, benzene, and the organometallic compound MMT, the molecular ion increases as I_{MS} decreases; this trend is the opposite of that observed for all of the other molecules. Finally, we see that most aromatic molecules produce C^+ ions readily, but benzene does not. These and many other observations may be the object of further in-depth studies.

3. Achieving Control with a Single Parameter. In this study, we have only evaluated a finite ($\sim 10^4$) number of differently phase-shaped pulses out of the possible 10^{200} different phase-shaped pulses that could be synthesized by our pulse shaper. This quantity is the number of permutations possible with 100 pixels and 100 different phase values per pixel. Despite the limited sampling, we consider that it is prudent to conclude that a single laser parameter such as I_{SHG} or I_{MS} can be used to determine the fragmentation pattern of a molecule. This is justified by the following arguments. First, the phases that were tested cover the most likely excitation pathways that could lead to influencing selective photochemistry. We evaluated different values of chirp and split pulses, which would mimic any pump−probe scenario involving higher and lower frequencies within the bandwidth of the pulse. We varied the period of a sine function, which would address the influence of pulse sequences that could coherently drive a vibrational frequency in the molecule. We varied the phase of a sinusoidal function, a parameter that is known to control multiphoton excitation. We evaluated binary phase functions, which cause large frequency-dependent changes in the amplitude of multiphoton excitation and produce complex pulse sequences that can selectively drive stimulated Raman transitions. We carried out a systematic evaluation for which the second-, third-, and fourth-order terms of the Taylor expansion parameters were varied systematically. Second, we also tested entire sets of random phases and random binary phases. However, as indicated in the text, the resulting photofragmentation from all of the different experiments was found to be related to the normalized I_{MS} or I_{SHG} values but independent of how the pulse was shaped.

Because I_{MS} is proportional to I_{SHG}, which is roughly inversely proportional to the duration of the pulse, we can refine our model to one in which the pulse duration is the single parameter that determines the extent of fragmentation in a molecule subjected to a strong near-IR field. Because some pulses are highly modulated in the time domain, their time duration can be estimated from I_{SHG}. In support of our statement, we point to the results in Figure 11b where we changed the pulse duration by restricting the bandwidth of the pulse. In that case, we saw changes in the ratio between the heavier and lighter mass fragments, just like when phase modulation was used. Therefore, our findings support the conclusion that the extent of fragmentation, which depends monotonically on I_{MS} and I_{SHG}, depends mainly on the pulse duration. It follows that the observed results for 16 different compounds can be understood in terms of prompt field ionization with subsequent multiphoton fragmentation processes, as stated earlier for *p*-NT fragmentation.

We would like to avoid the possible confusion between pulse duration and peak intensity. Peak intensity depends on three parameters: pulse energy, pulse duration, and focusing. In section II.4, we demonstrated how the fragmentation pattern was independent of focusing and hence peak intensity. In that case, we increased the diameter of the focal spot by one order of magnitude, without affecting the ratio between two fragments. In section III.4, we showed ample experimental evidence that fragmentation pathway does not depend on pulse energy. In those experiments, we showed that the fragmentation patterns

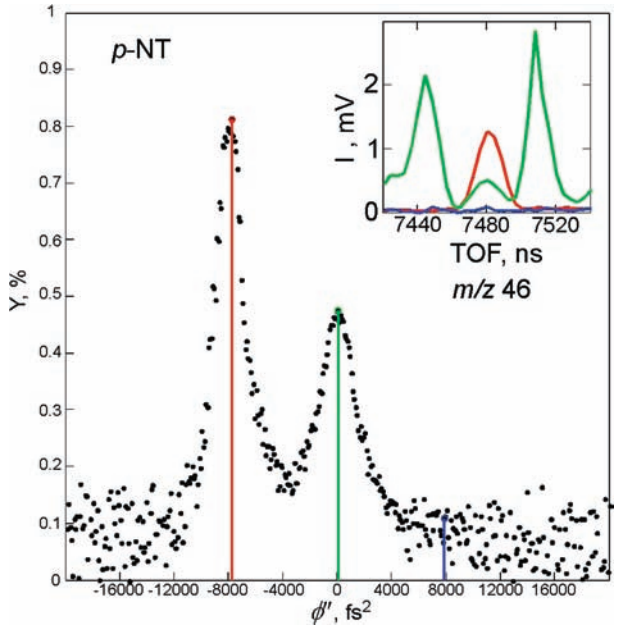

Figure 26. Unusual dependence of the relative yield of fragment *m*/*z* 46 from *p*-NT as a function of quadratic phase modulation. Inset: Mass spectra in the *m*/*z* 46 region for negative, zero, and positive chirp (red, green, and blue lines, respectively). The signal recorded with TL pulses has three features—a signature of dissociation from a doubly charged precursor. Note that the relative integrated intensity of these three lines (*Y*) is less than 1% from integrated yields of all ions.

as a function of four different pulse shaping functions did not change as we changed the laser pulse energy from 25 to 170 μJ. In section III.1, we showed that lengthening of the pulse by reducing its bandwidth led to changes in the fragmentation pattern as measured by the ratio between two masses. In the rest of the phase shaping experiments presented throughout this article, the overwhelming data support our observation that pulse duration, not peak intensity, caused the desired measure of selectivity.

Our findings are not entirely surprising. The dependence of fragmentation on pulse duration was observed at least two decades ago. In the early days, only two points were available, nanosecond versus picosecond laser pulses.[100−102] More importantly, the observation that mass spectrum fragmentation patterns change with chirp was independently found by several research groups working with femtosecond lasers. In 1998, Pastirk et al. showed that chirp could be used to enhance the concerted elimination of I_2 from CH_2I_2.[10] Levis et al. found that the fragmentation of *p*-nitroaniline changed substantially as a function of chirp.[20] However, the highlight of that article was that closed-loop control was capable of more sophisticated control compared to that of chirp. Jones et al. studied the chirp dependence on the fragmentation of S_8 and then used a closed-loop learning algorithm approach. He found that smaller fragments were produced with longer pulses and that the same dependence was found using the learning algorithm.[30] A more recent study on the open- and closed-loop dissociative ionization of ethanol by Yazawa et al.[37] found that a systematic approach, simple chirp, or pulse sequences yielded the best results. The overall pulse duration was found to be the essential factor for determining the relative yield and that the spike-like temporal profiles within a pulse did not affect the yield.[37]

If the complex time−frequency properties of the shaped near-IR pulses could direct energy flow or coherently driven a vibrational wave packet, causing bond-selective fragmentation and ionization in these experiments, we would have found at least one pulse producing a very different fragmentation ratio than that found in Figure 15, but we did not. Therefore, we find no evidence in all of our data that complex pulses could be used to achieve coherent bond-selective chemistry, thereby causing the exclusive formation of a desired fragment ion. The results shown in Figure 15, for instance, could be misinterpreted given that there is almost a factor of two difference between the lowest and highest ratio. However, the values are well within the Gaussian noise spectrum presented in Figure 15c, and the correct interpretation is that there was no control outside of what could be predicted given the value of I_{MS}.

If vibrational coherence played a role in the laser control experiments presented here, scanning the time between multiple subpulses in a shaped pulse should have revealed this type of coherence. Our measurements on different molecules presented in Figure 22, comparing a sinusoidal modulation with linear chirp, were designed to probe vibrational coherence. However, there was no instance where such a vibrational resonance was observed in any of the molecules studied. We take this experimental evidence to mean that vibrational coherence does not play a role in the fragmentation process.

In the language of learning algorithms, if there is an optimal solution and there is a gradient toward this solution, the search space is dubbed convex. Convex problems are easily solved by learning algorithms as well as by other gradient methods. Here, we argue that laser-controlled fragmentation under the conditions considered here can be represented as a convex problem. Minimum fragmentation corresponds to TL pulses, while maximum fragmentation corresponds to the longest pulses accessible by the pulse shaper. This observation may explain why learning-algorithm-based searches have been able to advance successfully despite the enormous search space and the experimental noise associated with molecular fragmentation as discussed here. If the search space was more like a needle-in-the-haystack, where one or more shaped pulses are greatly more optimal than all others, even those that are quite similar, then learning-algorithm-based searches would have greater difficulty optimizing different product yields. Given that the number of phase-shaped pulses that can produce a given value of ionization probability grows exponentially as I_{MS} approaches zero, a random search quickly finds a pulse with minimal—close to the noise level—ionization yield.

Despite all of the evidence shown, it may not be obvious why fragmentation and ionization do not seem to depend on parameters such as the time delay between subpulses. The primary reason is that there is a ~9 eV energy barrier that needs to be surmounted to achieve ionization of the molecules. The laser intensity needed for ionization causes excitation in a large number of intermediate rovibronic states, some of which include dissociation continua. Therefore, the resulting coherent superposition undergoes very fast delocalization, and we lose the ability to observe wave packet revivals as are observed in pump−probe experiments involving a single electronic state.

4. Observation of a Coherent Pathway. Until now, we have discussed the fate of the majority of the fragment ions, >98%, observed in laser fragmentation experiments. Having ruled out the coherent interaction between the laser and the molecule as the reason for observed changes in the fragmentation patterns, we are able to bring our attention to the few fragments, with yields typically in the few percent range, that become visible only with an excellent signal-to-noise ratio. In these cases, we have found a few examples for pathways that exhibit great sensitivity to the phase function, however these are restricted

to small single-charged ions resulting from multiply ionized species observed for the highest laser intensities. We therefore make the distinction between coherent control of fragmentation, for which we find no evidence, and coherent control of multiple ionization and subsequent fragmentation discussed here. In Figure 26, we present the chirp dependence on the relative yield of *m*/*z* 46 (NO_2^+). Notice that for positive chirps, we see the expected decrease in yield as chirp increases. However, for negative chirps, we find a very sharp maximum at -8000 fs^2, with a yield that is almost twice that found for TL pulses, an order of magnitude greater than would expected. Upon close analysis of the mass spectrum, we find that this mass, as well as a couple of others in *p*-NT, show a splitting (see Figure 26 insert) that is caused by high-energy dissociation (some fragments moving toward and some away from the detector). We interpret this enhancement and the corresponding line shapes as a dynamic process for which there is a field which optimizes secondary ionization to form *p*-NT^{++}, causing the prompt elimination of NO_2^+. The strong Coulombic repulsion results in the high kinetic energy, which results in the peak splitting. A similar pathway producing CH_3^+ is observed in acetophenone.[103] Details about this process and the molecules for which it is observed will be reported elsewhere.[104]

IV. Conclusion

In this article, we have addressed the prospects of laser-controlled chemistry resulting from the interaction between isolated molecules and strong ($10^{14}-10^{16}$ W/cm^2) nonresonant laser pulses shaped by different phase and amplitude functions. We find extensive (order of magnitude) control over the relative yield of product ions. Detailed analysis of the systematic experimental results has ledus to uncover a number of trends.

We find a one-to-one correspondence between the total ion yield and the total SHG generated by the shaped pulses. This correspondence allows us to compare results from differently shaped pulses. We find that the mass spectrum for any given shaped pulse also has a one-to-one correspondence with the total ion yield, independent of pulse shaping function. To demonstrate this correspondence, we plotted the mass spectra resulting when *p*-NT is fragmented by differently chirped pulses in a three-dimensional plot shown in Figure 27. The relative ion yields are outlined by the surface, which shows order-of-magnitude laser control over the fragmentation pattern. However, if we consider bond selective control of chemical reactions to be the ability to selectively cause the yield a particular ion exceed the yield of all other ions such that the mass spectrum collapses to a single *m*/*z* value, then we find no evidence in our data for bond selective control. Figure 27 contains experimental results for a number of very different phase functions. Notice that for the different phase functions we obtain the same surface, all points lie near the surface obtained for chirped pulses. Therefore, we find no shaped pulse capable of causing a fragmentation pattern that deviates from the mass spectra traced by the surface shown in Figure 27. We find that this conclusion applies to all the molecules studied here, and to all the different shaped pulses tested. This leads us to conclude that the fragmentation patterns observed are not sensitive to the details (amplitude and phase) of the shaped pulses, but depend on a single parameter such as the average pulse duration. This would explain the dependence on the integrated SHG.

To determine the laser fragmentation pattern for a given molecule with shaped intense fields, one needs a limited number of experiments to define its corresponding control surface. There is no need to evaluate the astronomical number of possible

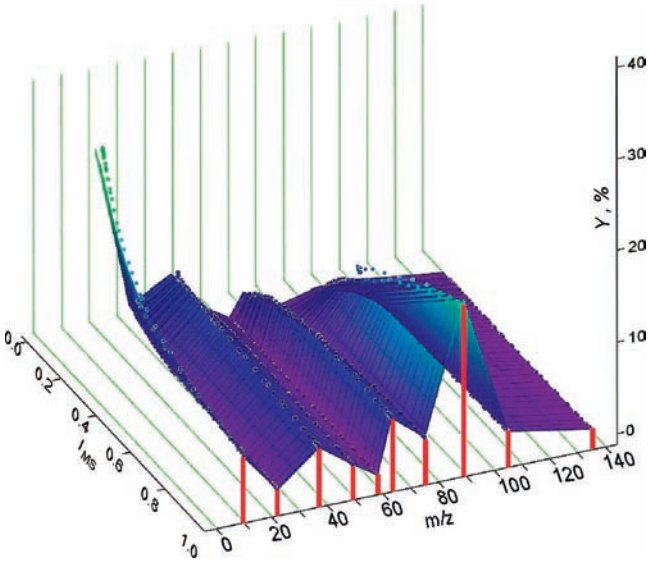

Figure 27. Laser control fragmentation surface for *p*-NT. The three-dimensional figure is generated by plotting the mass spectra obtained for different total ion yield values. The surface is given by the relative yield of the main ion peaks measured as a function of positive chirp. The points shown belong to additional experimental measurements, using different sinusoidal phase functions and by changing the time between two pulses formed by the redder and bluer frequencies of the laser.

shaped pulses that can be synthesized experimentally by the pulse shaper. The extent of fragmentation appears to depend on the laser−molecule interaction time. This observation is consistent with the absorption−ionization−dissociation mechanism. At our intensities, field ionization takes place first, and shaped pulses enhance fragmentation, producing cations that decrease in size following a photofragmentation sequence while the field is present.

To avoid misinterpretations of our conclusions, we should mention that our findings are valid for amplified near-IR phase-shaped femtosecond laser pulses on isolated molecules. Our observations are also restricted by the fact that we only monitor the nascent ions; therefore, we cannot determine the fate of the neutrals. We have also pointed out that for some ions resulting from multiple ionization pathways in some molecules, we observe that the product yield is highly sensitive to the time−frequency details of the shaped pulse. We stress that these pathways affect very few (one or two) of the product ions observed, and their relative yield is small even when optimized. The majority of the fragments are formed by an incoherent process that depends mainly on pulse duration and not on the precise phase structure of the pulse. Therefore we find no evidence for bond-selective coherent control of chemical reactions induced by the shaped pulses. We do find the signature of coherent control of a multiple ionization pathway.

Although our experiments indicate that laser control of chemical reactions with a single intense near-IR pulse is limited within the laser control fragmentation surface, as illustrated in Figure 27 for *p*-NT, one may argue that there ought to be at least one class of pulses capable of achieving selective bond cleavage, well above the statistical noise, and thus generating a fragmentation pattern that significantly deviates from the laser control fragmentation surface. Experimentally refuting the existence of such a class of pulses would take an infinite number of experiments given the essentially infinite resolution that can be achieved by the pulse shaper. Realistically, the bandwidth of the pulses is limited, the number of pixels is limited, the noise of the experiment makes minute changes in phase

immeasurable, and the experimental time scale is also limited. The molecular system has a finite coherence lifetime and a finite initial distribution of states that also place limits on the degree of finesse that would make sense to explore. All that we know at this time is that all of the experiments that have been shown here show no deviation from the laser control fragmentation surface; by this, we mean that the fragmentation observed for any shaped pulse is very similar to that found for a positively chirped pulse that creates an equivalent total ion yield. We emphasize that the shaped pulses in our experiments were chosen to represent an extremely diverse set, and to probe as many potential mechanisms as possible. Accordingly, the present study promises a robust method for controlling molecular fragmentation, with potential analytic and synthetic applications.

After a thorough examination of the influence of different sets of experiments on the effects of phase- and amplitude-shaped pulses on a molecular fragmentation, we can claim to know everything (or at least something) we always wanted to know about laser control of molecular dissociation. We were afraid to find that coherence plays a minor role in the fragmentation of isolated molecules by shaped near-IR pulses, and this is exactly what we found. This implies that electronic and vibrational coherence seem to dissipate through wave packet delocalization and have minimal influence on the photofragmentation pathways. Although we found that fragmentation cannot be controlled coherently, the large changes in the fragment ion yields suggest new systematic approaches to laser control of chemical reactions.

Acknowledgment. We are grateful to Professors Gustav Gerber, Itzik Ben-Itzhak and Robert Jones for discussions on the role of volume effects in high-intensity laser photochemistry. We gratefully acknowledge the partial financial support for our study of molecules in high-intensity laser fields from the Chemical Sciences, Geosciences and Biosciences Division, Office of Basic Energy Sciences, Office of Science, U.S. Department of Energy, and from the NSF (CHE-0500661) supporting our systematic study of laser control of chemical reactions. This work is also supported by an STTR subcontract from BioPhotonic Solutions, Inc., funded by the U.S. Army Research Office (the content of the information does not necessarily reflect the position or the policy of the Government; no official endorsement should be inferred).

References and Notes

(1) Rousseau, D. L. *J. Chem. Educ.* **1966**, *43*, 566.
(2) Zewail, A. H. *Phys. Today* **1980**, *33*, 27.
(3) Zewail, A. H. *Femtochemistry: Ultrafast Dynamics of the Chemical Bond*; World Scientific: River Edge, NJ, 1994; Vol. 1.
(4) Zewail, A. H. *Femtochemistry: Ultrafast Dynamics of the Chemical Bond*; World Scientific: River Edge, NJ, 1994; Vol. 2.
(5) Zewail, A. H. *Femtochemistry: Ultrafast Dynamics of the Chemical Bond*; World Scientific: River Edge, NJ, 1994; Vol. 3.
(6) Tannor, D. J.; Rice, S. A. *J. Chem. Phys.* **1985**, *83*, 5013.
(7) Brumer, P.; Shapiro, M. *Chem. Phys. Lett.* **1986**, *126*, 541.
(8) Tannor, D. J.; Kosloff, R.; Rice, S. A. *J. Chem. Phys.* **1986**, *85*, 5805.
(9) Krause, J. L.; Whitnell, R. M.; Wilson, K. R.; Yan, Y. J.; Mukamel, S. *J. Chem. Phys.* **1993**, *99*, 6562.
(10) Pastirk, I.; Brown, E. J.; Zhang, Q. G.; Dantus, M. *J. Chem. Phys.* **1998**, *108*, 4375.
(11) Manz, J. Molecular Wavepacket Dynamic: Theory for Experiments 1926−1996. In *Femtochemistry and Femtobiology: Ultrafast Reaction Dynamics at Atomic-Scale Resolution*; Sundstrum, V., Ed.; Imperial College Press: London, 1996; p 80.
(12) Brixner, T.; Gerber, G. *ChemPhysChem* **2003**, *4*, 418.
(13) Dantus, M.; Lozovoy, V. V. *Chem. Rev.* **2004**, *104*, 1813.
(14) Assion, A.; Baumart, T.; Bergt, M.; Brixner, T.; Kiefer, B.; Sayfried, V.; Strehle, M.; Gerber, G. *Science* **1998**, *282*, 919.
(15) Bergt, M.; Brixner, T.; Kiefer, B.; Strehle, M.; Gerber, G. *J. Phys. Chem. A* **1999**, *103*, 10381.
(16) Brixner, T.; Kiefer, B.; Gerber, G. *Chem. Phys.* **2001**, *267*, 241.
(17) Bergt, M.; Brixner, T.; Dietl, C.; Kiefer, B.; Gerber, G. *J. Organomet. Chem.* **2002**, *661*, 199.
(18) Brixner, T.; Damrauer, N. H.; Krampert, G.; Niklaus, P.; Gerber, G. *J. Mod. Opt.* **2003**, *50*, 539.
(19) Levis, R. J.; Menkir, G. M.; Rabitz, H. *Science* **2001**, *292*, 709.
(20) Levis, R. J.; Rabitz, H. A. *J. Phys. Chem. A* **2002**, *106*, 6427.
(21) Graham, P.; Menkir, G.; Levis, R. J. *Spectrocim. Acta, Part B* **2003**, *58*, 1097.
(22) Daniel, C.; Full, J.; Gonzalez, L.; Kaposta, C.; Krenz, M.; Lupulescu, C.; Manz, J.; Minemoto, S.; Oppel, M.; Rosendo-Francisco, P.; Vajda, S.; Wöste, L. *Chem. Phys.* **2001**, *267*, 247.
(23) Daniel, C.; Full, J.; Gonzalez, L.; Lupulescu, C.; Manz, J.; Merli, A.; Vajda, S.; Wöste, L. *Science* **2003**, *299*, 536.
(24) Cardoza, D.; Langhojer, F.; Trallero-Herrero, C.; Monti, O. L. A.; Weinacht, T. *Phys. Rev. A* **2004**, *70*, 053406.
(25) Langhojer, F.; Cardoza, D.; Baertschy, M.; Weinacht, T. *J. Chem. Phys.* **2005**, *122*, 014102.
(26) Cardoza, D.; Baertschy, M.; Weinacht, T. *Chem. Phys. Lett.* **2005**, *411*, 311.
(27) Cardoza, D.; Trallero-Herrero, C.; Langhojer, F.; Rabitz, H.; Weinacht, T. *J. Chem. Phys.* **2005**, *122*, 124306.
(28) Cardoza, D.; Pearson, B. J.; Baertschy, M.; Weinacht, T. *J. Photochem. Photobiol., A* **2006**, *180*, 277.
(29) Cardoza, D.; Baertschy, M.; Weinacht, T. *J. Chem. Phys.* **2005**, *123*, 074315.
(30) Wells, E.; Betsch, K. J.; Conover, C. W. S.; DeWitt, M. J.; Pinkham, D.; Jones, R. R. *Phys. Rev. A* **2005**, *72*, 063406.
(31) Judson, R. S.; Rabitz, H. *Phys. Rev. Lett.* **1992**, *68*, 1500.
(32) Pastirk, I.; Kangas, M.; Dantus, M. *J. Phys. Chem. A* **2005**, *109*, 2413.
(33) Shane, J. C.; Lozovoy, V. V.; Dantus, M. *J. Phys. Chem. A* **2006**, *110*, 11388.
(34) Lozovoy, V. V.; Dantus, M. *ChemPhysChem* **2005**, *6*, 1970.
(35) Lozovoy, V. V.; Gunaratne, T. C.; Shane, J. C.; Dantus, M. *ChemPhysChem* **2006**, *7*, 2471.
(36) Lozovoy, V., V.; Dantus, M. *Annu. Rep. Prog. Chem., Sect. C: Phys. Chem.* **2006**, *102*, 227.
(37) Yazawa, H.; Tanabe, T.; Okamoto, T.; Yamanaka, M.; Kannari, F.; Itakura, R.; Yamanouchi, K. *J. Chem. Phys.* **2006**, *124*, 204314.
(38) Itakura, R.; Yamanouchi, K.; Tanabe, T.; Okamoto, T.; Kannari, F. *J. Chem. Phys.* **2003**, *119*, 4179.
(39) Mathur, D.; Rajgara, F. A. *J. Chem. Phys.* **2004**, *120*, 5616.
(40) Dela Cruz, J. M.; Lozovoy, V. V.; Dantus, M. *J. Phys. Chem. A* **2005**, *109*, 8447.
(41) Pastirk, I.; Lozovoy, V., V.; Dantus, M. *Appl. Optics* **2006**, *46*, 4041.
(42) Kosmidis, C.; Marshall, A.; Clark, A.; Deas, R. M.; Ledingham, K. W. D.; Singhal, R. P. *Rapid Commun. Mass Spectrom.* **1994**, *8*, 607.
(43) Ledingham, K. W. D.; Kilic, H. S.; Kosmidis, C.; Deas, R. M.; Marshall, A.; McCanny, T.; Singhal, R. P.; Langley, A. J.; Shaikh, W. *Rapid Commun. Mass Spectrom.* **1995**, *9*, 1522.
(44) Kosmidis, C.; Ledingham, K. W. D.; Kilic, H. S.; McCanny, T.; Singhal, R. P.; Langley, A. J.; Shaikh, W. *J. Phys. Chem. A* **1997**, *101*, 2264.
(45) Tasker, A. D.; Robson, L.; Ledingham, K. W. D.; McCanny, T.; Hankin, S. M.; McKenna, P.; Kosmidis, C.; Jaroszynski, D. A.; Jones, D. R. *J. Phys. Chem. A* **2002**, *106*, 4005.
(46) *NIST Standard Reference Database Number 69*, June 2005 Release; National Institute of Standards and Technology: Bethesda, MD, 2005.
(47) Abbott, J. E.; Peng, X. Z.; Kong, W. *J. Chem. Phys.* **2002**, *117*, 8670.
(48) Sheng, L. S.; Wu, G. H.; Gao, H.; Zhang, Y. W. *Chem. J. Chin. Univ.* **1997**, *18*, 2041.
(49) Pastirk, I.; Resan, B.; Fry, A.; MacKay, J.; Dantus, M. *Opt. Express* **2006**, *14*, 9537.
(50) Dantus, M.; Lozovoy, V. V.; Pastirk, I. *Laser Focus World* **2007**, 101.
(51) Xu, B. W.; Gunn, J. M.; Dela Cruz, J. M.; Lozovoy, V. V.; Dantus, M. *J. Opt. Soc. Am. B* **2006**, *23*, 750.
(52) Lozovoy, V. V.; Pastirk, I.; Dantus, M. *Opt. Lett.* **2004**, *29*, 775.
(53) Walowicz, K. A.; Pastirk, I.; Lozovoy, V. V.; Dantus, M. *J. Phys. Chem. A* **2002**, *106*, 9369.
(54) Lozovoy, V. V.; Pastirk, I.; Walowicz, K. A.; Dantus, M. *J. Chem. Phys.* **2003**, *118*, 3187.
(55) Cerullo, G.; Bardeen, C. J.; Wang, Q.; Shank, C. V. *Chem. Phys. Lett.* **1996**, *262*, 362.
(56) Wohlleben, W.; Buckup, T.; Herek, J. L.; Motzkus, M. *ChemPhysChem* **2005**, *6*, 850.
(57) Meshulach, D.; Silberberg, Y. *Nature* **1998**, *396*, 239.

(58) Dela Cruz, J. M.; Pastirk, I.; Lozovoy, V. V.; Walowicz, K. A.; Dantus, M. *J. Phys. Chem. A* **2004**, *108*, 53.
(59) Comstock, M.; Lozovoy, V. V.; Pastirk, I.; Dantus, M. *Opt. Express* **2004**, *12*, 1061.
(60) Lozovoy, V. V.; Shane, J. C.; Xu, B. W.; Dantus, M. *Opt. Express* **2005**, *13*, 10882.
(61) Lozovoy, V. V.; Xu, B. W.; Shane, J. C.; Dantus, M. *Phys. Rev. A* **2006**, *74*, 041805.
(62) Tang, X. P.; Becker, A.; Liu, W.; Sharifi, S. M.; Kosareva, O. G.; Kandidov, V. P.; Agostini, P.; Chin, S. L. *Appl. Phys. B* **2005**, *80*, 547.
(63) Muller, A. M.; Uiterwaal, C.; Witzel, B.; Wanner, J.; Kompa, K. L. *J. Chem. Phys.* **2000**, *112*, 9289.
(64) Fraser, G. W. *Int. J. Mass Spectrom.* **2002**, *215*, 13.
(65) Krems, M.; Zirbel, J.; Thomason, M.; DuBois, R. D. *Rev. Sci. Instrum.* **2005**, *76*.
(66) Hankin, S. M.; Villeneuve, D. M.; Corkum, P. B.; Rayner, D. M. *Phys. Rev. A* **2001**, *64*, 013405.
(67) Uiterwaal, C.; Gebhardt, C. R.; Schroder, H.; Kompa, K. L. *Eur. Phys. J. D* **2004**, *30*, 379.
(68) Posthumus, J. H. *Rep. Prog. Phys.* **2004**, *67*, 623.
(69) Watson, J. T. *Introduction to Mass Spectrometry*, 3rd ed.; Lippincott-Raven: Philadelphia, PA, 1997.
(70) Robson, L.; Ledingham, K. W. D.; McKenna, P.; McCanny, T.; Shimizu, S.; Yang, J. M.; Wahlstrom, C. G.; Lopez-Martens, R.; Varju, K.; Johnsson, P.; Mauritsson, J. *J. Am. Soc. Mass Spectrom.* **2005**, *16*, 82.
(71) Zhang, L.; Frasinski, L. J.; Codling, K. *J. Phys. B: At. Mol. Opt. Phys.* **1994**, *27*, 3427.
(72) Hankin, S. M.; Villeneuve, D. M.; Corkum, P. B.; Rayner, D. M. *Phys. Rev. Lett.* **2000**, *84*, 5082.
(73) Wang, P. Q.; Sayler, A. M.; Carnes, K. D.; Esry, B. D.; Ben-Itzhak, I. *Opt. Lett.* **2005**, *30*, 664.
(74) Lozovoy, V. V.; Xu, B.; Shane, J. C.; Dantus, M. *Phys. Rev. A* **2006**, *74*, 041805.
(75) Dela Cruz, J. M.; Lozovoy, V. V.; Dantus, M. *J. Mass Spectrom.* **2007**, *42*, 178.
(76) Fuss, W.; Schmid, W. E.; Trushin, S. A. *J. Chem. Phys.* **2000**, *112*, 8347.
(77) Tonnies, K.; Schmid, R. P.; Weickhardt, C.; Reif, J.; Grotemeyer, J. *Int. J. Mass Spectrom.* **2001**, *206*, 245.
(78) Weickhardt, C.; Tonnies, K. *Rapid Commun. Mass Spectrom.* **2002**, *16*, 442.
(79) Zhu, X.; Gunaratne, T. C.; Lozovoy, V. V.; Dantus, M. *J. Phys. Chem. A* **2008**, accepted for publication.
(80) Bursey, M. M.; McLaffer. Fw. *J. Am. Chem. Soc.* **1966**, *88*, 5023.
(81) Brown, P. *Org. Mass Spectrom.* **1970**, *4*, 533.
(82) Beynon, J. H.; Bertrand, M.; Cooks, R. G. *J. Am. Chem. Soc.* **1973**, *95*, 1739.
(83) Harris, F. M.; Mukhtar, E. S.; Griffiths, I. W.; Beynon, J. H. *Proc. R. Soc. London, Ser. A* **1981**, *374*, 461.
(84) Baer, T.; Morrow, J. C.; Shao, J. D.; Olesik, S. *J. Am. Chem. Soc.* **1988**, *110*, 5633.
(85) Choe, J. C.; Kim, M. S. *J. Phys. Chem.* **1991**, *95*, 50.
(86) Cassady, C. J.; McElvany, S. W. *Org. Mass Spectrom.* **1993**, *28*, 1650.
(87) Lablanquie, P.; Ohashi, K.; Nishi, N. *J. Chem. Phys.* **1993**, *98*, 399.
(88) Panczel, M.; Baer, T. *Int. J. Mass Spectrom. Ion Process.* **1984**, *58*, 43.
(89) Nishimura, T.; Das, P. R.; Meisels, G. G. *J. Chem. Phys.* **1986**, *84*, 6190.
(90) Moini, M.; Eyler, J. R. *Int. J. Mass Spectrom. Ion Process.* **1987**, *76*, 47.
(91) Marshall, A.; Clark, A.; Jennings, R.; Ledingham, K. W. D.; Singhal, R. P. *Int. J. Mass Spectrom. Ion Process.* **1992**, *112*, 273.
(92) Osterheld, T. H.; Baer, T.; Brauman, J. I. *J. Am. Chem. Soc.* **1993**, *115*, 6284.
(93) Kosmidis, C.; Ledingham, K. W. D.; Clark, A.; Marshall, A.; Jennings, R.; Sander, J.; Singhal, R. P. *Int. J. Mass Spectrom. Ion Process.* **1994**, *135*, 229.
(94) Galloway, D. B.; Bartz, J. A.; Huey, L. G.; Crim, F. F. *J. Chem. Phys.* **1993**, *98*, 2107.
(95) Galloway, D. B.; Glenewinkelmeyer, T.; Bartz, J. A.; Huey, L. G.; Crim, F. F. *J. Chem. Phys.* **1994**, *100*, 1946.
(96) Hwang, W. G.; Kim, M. S.; Choe, J. C. *J. Phys. Chem.* **1996**, *100*, 9227.
(97) Brill, T. B.; James, K. J.; Chawla, R.; Nicol, G.; Shukla, A.; Futrell, I. H. *J. Phys. Org. Chem.* **1999**, *12*, 819.
(98) Cooper, L.; Shpinkova, L. G.; Rennie, E. E.; Holland, D. M. P.; Shaw, D. A. *Int. J. Mass Spectrom.* **2001**, *207*, 223.
(99) Gruebele, M.; Bigwood, R. *Int. Rev. Phys. Chem.* **1998**, *17*, 91.
(100) Yang, J. J.; Gobeli, D. A.; El Sayed, M. A. *J. Phys. Chem.* **1985**, *89*, 3426.
(101) Szaflarski, D. M.; El Sayed, M. A. *J. Phys. Chem.* **1988**, *92*, 2234.
(102) Weinkauf, R.; Aicher, P.; Wesley, G.; Grotemeyer, J.; Schlag, E. W. *J. Phys. Chem.* **1994**, *98*, 8381.
(103) Lozovoy, V., V.; Dantus, M. *Chem. Phys.* **2008**, in press.
(104) Zhu, X.; Lozovoy, V. V.; Dantus, M. *J. Phys. Chem. A* **2008**, in press.
(105) Anand, S.; Zamari, M. M.; Menkir, G.; Levis, R. J.; Schlegel, H. B. *J. Phys. Chem. A* **2004**, *108*, 3162.
(106) Singhal, R. P.; Kilic, H. S.; Ledingham, K. W. D.; Kosmidis, C.; McCanny, T.; Langley, A. J.; Shaikh, W. *Chem. Phys. Lett.* **1996**, *253*, 81.
(107) Itakura, R.; Watanabe, J.; Hishikawa, A.; Yamanouchi, K. *J. Chem. Phys.* **2001**, *114*, 5598.
(108) Harada, H.; Shimizu, S.; Yatsuhashi, T.; Sakabe, S.; Izawa, Y.; Nakashima, N. *Chem. Phys. Lett.* **2001**, *342*, 563.
(109) Harada, H.; Tanaka, M.; Murakami, M.; Shimizu, S.; Yatsuhashi, T.; Nakashima, N.; Sakabe, S.; Izawa, Y.; Tojo, S.; Majima, T. *J. Phys. Chem. A* **2003**, *107*, 6580.
(110) Trushin, S. A.; Fuss, W.; Schmid, W. E. *J. Phys. B: At. Mol. Opt. Phys.* **2004**, *37*, 3987.
(111) Ma, R.; Wu, C. Y.; Huang, J.; Xia, L.; Chen, J. X.; Yang, H.; Gong, Q. H. *Chem. Phys. Lett.* **2005**, *404*, 370.
(112) Ma, R.; Li, X.; Ren, H. Z.; Yang, H.; Jiang, H. B.; Gong, Q. H. *Int. J. Mass Spectrom.* **2005**, *242*, 43.
(113) Chen, J. X.; Ma, R.; Ren, H. Z.; Li, X.; Yang, H.; Gong, Q. H. *Int. J. Mass Spectrom.* **2005**, *241*, 25.
(114) Ren, H. Z.; Wu, C. Y.; Ma, R.; Yang, H.; Jiang, H. B.; Gong, Q. H. *Int. J. Mass Spectrom.* **2002**, *219*, 305.
(115) Sakai, H.; Larsen, J. J.; Wendt-Larsen, I.; Olesen, J.; Corkum, P. B.; Stapelfeldt, H. *Phys. Rev. A* **2003**, *67*, 063404.
(116) Bhardwaj, V. R.; Rayner, D. M.; Villenueve, D. M.; Corkum, P. B. *Phys. Rev. Lett.* **2001**, *87*, 253003.
(117) Rajgara, F. A.; Krishnamurthy, M.; Mathur, D. *Phys. Rev. A* **2003**, *68*, 023407.
(118) Rajgara, F. A.; Krishnamurthy, M.; Mathur, D. *J. Chem. Phys.* **2003**, *119*, 12224.
(119) Wang, S. F.; Tang, X. P.; Gao, L. R.; Elshakre, M. E.; Kong, F. N. *J. Phys. Chem. A* **2003**, *107*, 6123.
(120) Elshakre, M. E.; Gao, L. R.; Tang, X. P.; Wang, S. F.; Shu, Y. F.; Kong, F. N. *J. Chem. Phys.* **2003**, *119*, 5397.
(121) Wang, Y. Q.; Zhu, J. Y.; Wang, L.; Cong, S. L. *Int. J. Quantum Chem.* **2006**, *106*, 1138.
(122) Zhu, J. Y.; Guo, W.; Wang, Y. Q.; Wang, L. *Chem. Phys.* **2006**, *326*, 571.
(123) Levis, R. J.; DeWitt, M. J. *J. Phys. Chem. A* **1999**, *103*, 6493.
(124) DeWitt, M. J.; Levis, R. J. *J. Chem. Phys.* **1998**, *108*, 7045.
(125) Talebpour, A.; Bandrauk, A. D.; Yang, J.; Chin, S. L. *Chem. Phys. Lett.* **1999**, *313*, 789.
(126) Talebpour, A.; Bandrauk, A. D.; Vijayalakshmi, K.; Chin, S. L. *J. Phys. B: At. Mol. Opt. Phys.* **2000**, *33*, 4615.
(127) Ivanov, M.; Seideman, T.; Corkum, P.; Ilkov, F.; Dietrich, P. *Phys. Rev. A* **1996**, *54*, 1541.
(128) Kosmidis, C.; Kaziannis, S.; Siozos, P.; Lyras, A.; Robson, L.; Ledingham, K. W. D.; McKenna, P.; Jaroszynski, D. A. *Int. J. Mass Spectrom.* **2006**, *248*, 1.
(129) Trushin, S. A.; Fuss, W.; Schikarski, T.; Schmid, W. E.; Kompa, K. L. *J. Chem. Phys.* **1997**, *106*, 9386.
(130) Markevitch, A. N.; Romanov, D. A.; Smith, S. M.; Levis, R. J. *Phys. Rev. Lett.* **2004**, *92*, 063001.
(131) Markevitch, A. N.; Smith, S. M.; Romanov, D. A.; Schlegel, H. B.; Ivanov, M. Y.; Levis, R. J. *Phys. Rev. A* **2003**, *68*, 011402.
(132) Markevitch, A. N.; Romanov, D. A.; Smith, S. M.; Schlegel, H. B.; Ivanov, M. Y.; Levis, R. J. *Phys. Rev. A* **2004**, *69*, 013401.
(133) Lezius, M.; Blanchet, V.; Rayner, D. M.; Villeneuve, D. M.; Stolow, A.; Ivanov, M. Y. *Phys. Rev. Lett.* **2001**, *86*, 51.
(134) Lezius, M.; Blanchet, V.; Ivanov, M. Y.; Stolow, A. *J. Chem. Phys.* **2002**, *117*, 1575.